Two-component doublet-triplet scalar dark matter stabilizing the electroweak vacuum

Nabarun Chakrabarty,[1,2,*] Rishav Roshan,[3,†] and Arunansu Sil[3,‡]

[1]*Department of Physics, Indian Institute of Technology Kanpur, Kanpur, Uttar Pradesh 208016, India*
[2]*Centre for High Energy Physics, Indian Institute of Science, C.V. Raman Avenue, Bangalore 560012, India*
[3]*Department of Physics, Indian Institute of Technology Guwahati, Assam-781039, India*

(Received 19 February 2021; accepted 13 May 2022; published 7 June 2022)

A two-component scalar dark matter scenario comprising an additional scalar doublet and a $Y = 0$ scalar triplet is proposed. Key features of the ensuing dark matter phenomenology are highlighted with emphasis on interconversion between the two dark matter components. For suitable choices of the model parameters, we show that such interconversion can explain the observed relic abundance when the doublet dark matter component has mass in the *desert* region while the triplet component has sub-TeV mass. This finding is important in the context of such mass regions known to predict underabundant relic density for the stand-alone cases of the scalar doublet and triplet. In addition, we also show that the present scenario can stabilize the electroweak vacuum up to the Planck scale in the parameter space responsible for the requisite dark matter observables.

DOI: 10.1103/PhysRevD.105.115010

I. INTRODUCTION

The discovery of a Higgs boson at the Large Hadron Collider (LHC) [1,2] completes the particle spectrum of the Standard Model (SM). Moreover, the interactions of the discovered boson to fermions and gauge bosons are in good agreement with the SM predictions. Despite this success, certain shortcomings of the SM on both theoretical and experimental fronts keep the hope for additional dynamics alive and kicking. That the SM alone cannot predict a stable electroweak (EW) vacuum up to the Planck scale for a t-quark pole mass at the upper end of its allowed band counts as one such theoretical shortcoming. That is, the SM quartic coupling turns negative while evolving under the renormalization group (RG), thereby destabilizing the vacuum, and the energy scale where that happens is dictated by the t-quark mass chosen [3–7]. However, augmenting the SM by additional bosonic degrees of freedom (see [8–24] for a partial list) can help the Higgs quartic coupling overcome the destabilizing effect coming dominantly from the t quark. This motivates one to look for extensions of the SM scalar sector. On the experimental front, the SM alone cannot postulate a dark matter (DM) candidate, something whose existence is collectively hinted at by observation of galactic rotation curves [25], gravitational lensing [26], and anisotropies in the cosmic microwave background. Hitherto, the only information known about DM is its relic abundance, and it is precisely determined by experiments studying anisotropies in cosmic microwave background radiation like Wilkinson Microwave Anisotropy Probe [27] and *PLANCK* [28]. Since these experiments do not shed light on DM spin, the possibility that DM can either be a scalar, a fermion, or a vector boson remains open.

Some attractive scalar DM scenarios are based on augmenting the SM scalar sector by additional scalar $SU(2)_L$ multiplets. The most minimal case which, in fact, transforms trivially under $SU(2)_L$ is that of a scalar singlet (an updated analysis is Ref. [29]). However, this scenario interacts with the SM only through the Higgs portal and is tightly constrained. The only mass regions where the scalar singlet accounts for all the observed amount of DM are the Higgs resonance dip and the $\sim$1 TeV region, with the former being extremely fine-tuned. We, therefore, focus on the higher $SU(2)_L$ multiplets henceforth that feature gauge interactions.

The next minimal multiplet is an $SU(2)_L$ doublet. This is the popular inert doublet model (IDM) whose neutral CP-even or CP-odd component can serve as a DM candidate [30–42]. Despite the popularity, an aesthetically dissatisfying feature of the IDM is the existence of the $M_{\rm DM} \in [M_W, 500\ {\rm GeV}]$ region, henceforth called the *desert* region,

*nabarunc@iitk.ac.in
†rishav.roshan@iitg.ac.in
‡asil@iitg.ac.in

which otherwise would have been an interesting range to explore experimentally, wherein only an underabundant thermal relic density is observed. This underabundance in the desert region is observed precisely because of the DM annihilating to the SM gauge bosons with a huge annihilation cross section. However, for $M_{\rm DM} \geq 500$ GeV, small mass splittings between the inert scalars, and an appropriate value for the DM-Higgs portal interaction, the IDM can indeed predict the observed relic abundance. This can be further traced back to cancellations that are triggered between the s-channel, t-channel, and contact interaction terms of the DM DM $\to VV$ amplitude for such near degeneracy. And, in this fashion, the DM $\to VV$ annihilation cross section attains the right value for $M_{\rm DM} \geq 500$ GeV so as to predict a $\simeq$0.1 relic density. There have been efforts in the recent past to revive the IDM desert region by augmenting the IDM with additional fields. Some examples involving additional bosons are Ref. [43] (an additional scalar singlet) and Refs. [44–50] (an additional scalar doublet); while examples involving additional fermions are Refs. [51,52] (right-handed neutrinos). With the scalar singlet and doublet extensions of the IDM already in place, an interesting exercise could be to try extending by a scalar $SU(2)_L$ triplet. And we choose to take one with $Y = 0$ in this study, since it is the most minimal scalar triplet in terms of particle content.

A stand-alone $Y = 0$ scalar triplet itself can also be a prospective dark multiplet in the inert limit [53–61]. A crucial difference between the inert triplet model (ITM) and the IDM is that the former features near-degenerate charged and neutral scalars (the mass splitting being 166 MeV only). In addition to cancellations in DM $\to VV$, there are also compulsory coannihilations as a fallout of this near degeneracy. Therefore, for the model to generate the requisite thermal relic abundance and evade the latest direct detection bound, the DM scalar has to at least have $M_{\rm DM} \simeq 1.8$ TeV. A wider desert region is thus observed in comparison to the IDM. Therefore, committing to the $Y = 0$ scalar triplet scenario annuls the possibility of having of sub-TeV DM. Studies on the stability of the EW vacuum in an IDM and ITM are Refs. [12,56,57,62]. We mention here that there is likewise the possibility of populating the triplet desert region by injecting additional fields into the theory [63].

Since the quantum number(s) of DM cannot be inferred from fundamental principles or available experimental data, the possibility that DM consists of more than one type of particle remains alive. Such a notion was first proposed in Ref. [64] and has, in turn, spurred many investigations thereafter, a representative list being Refs. [43,44,52,54,63,65–89]. Such multiparticle DM frameworks open up enticing DM-DM conversion processes that contribute to the thermal relic abundance but not to DM-nucleon scattering as looked for in the direct detection (DD) experiments [90–93]. A multipartite DM scenario, therefore, can evade the ever-tightening bound on the DD rates while enlarging the parameter space compatible with the observed relic density. We propose one such multicomponent DM framework in this work that combines the two single-component scenarios discussed above, i.e., an inert scalar doublet and a $Y = 0$ scalar triplet. The key takeaway from the discussion on the IDM and ITM is that certain mass regions in both cases predict underabundant relic densities precisely due to the gauge interaction-mediated co(annihilations). We aim to investigate here if DM-DM conversion can revive these mass regions in the proposed multicomponent setup. In other words, the primary motive of this study is to revive the DM mass regions corresponding to the two $SU(2)_L$ multiplets that are forbidden in the respective stand-alone cases. Since these inert multiplets interact with the SM-like doublet via the scalar potential, they tend to aid to EW vacuum stability by generating positive contributions to the RG running of the SM-like quartic coupling. Therefore, we also wish to find out if the parameter space compatible with DM relic density and DD can stabilize the EW vacuum till the Planck scale.

This study is organized as follows. The model is detailed in Sec. II, and the relevant constraints are discussed in Sec. III. Section IV throws light on the multicomponent DM phenomenology with an emphasis on DM-DM conversion. Section V discusses EW vacuum (meta)stability and comments on the results obtained upon demanding the DM constraints and a (meta)stable vacuum up to the Planck scale together. We conclude in Sec. VI. Important formulas are relegated to the Appendix.

II. MODEL

In the present study, we extend the SM by an $SU(2)_L$ scalar doublet Φ with $Y = \frac{1}{2}$ and a hyperchargeless $SU(2)_L$ scalar triplet $\mathcal{T}$. A discrete symmetry $Z_2 \times Z_2'$ is introduced under which the SM fields are trivial while the additional scalar multiplets are charged. We provide in Table I the quantum numbers of all the scalars in the scenario under both gauge and discrete symmetries. The $Z_2 \times Z_2'$ ensures stability of the newly introduced scalar multiplets as a result of which the neutral scalars, if lightest within their respective multiplets, can be DM candidates. Therefore, the present setup can accommodate a two-component DM scenario. We add that Φ ($\mathcal{T}$) hereafter can be referred to as an *inert* doublet (triplet), since it does not pick up a vacuum expectation value (VEV) by virtue of the discrete symmetry.

TABLE I. Quantum numbers of the SM Higgs doublet H and the inert multiplets Φ and $\mathcal{T}$.

Particle	$SU(2)$	$U(1)_Y$	Z_2	Z_2'
H	2	$\frac{1}{2}$	+	+
Φ	2	$\frac{1}{2}$	+	−
$\mathcal{T}$	3	0	−	+

The most general renormalizable scalar potential consistent with $SU(2)_L \times U(1)_Y \times Z_2 \times Z_2'$ for the given scalar content, $V(H, \Phi, \mathcal{T})$, consists of (i) V_H, terms involving H alone; (ii) V_Φ, terms involving Φ alone; (iii) $V_\mathcal{T}$, terms involving $\mathcal{T}$ alone; and (iv) $V_{\rm int}$, interactions involving all H, Φ, and $\mathcal{T}$. That is,

$$V(H,\Phi,\mathcal{T}) = V_H + V_\Phi + V_\mathcal{T} + V_{\rm int}, \tag{1}$$

where

$$V_H = -\mu_H^2 H^\dagger H + \lambda_H (H^\dagger H)^2, \tag{2a}$$

$$V_\Phi = \mu_\Phi^2 \Phi^\dagger \Phi + \lambda_\Phi (\Phi^\dagger \Phi)^2, \tag{2b}$$

$$V_\mathcal{T} = \frac{M_T^2}{2}\mathrm{Tr}[\mathcal{T}^2] + \frac{\lambda_T}{4!}(\mathrm{Tr}[\mathcal{T}^2])^2, \tag{2c}$$

and

$$\begin{aligned} V_{\rm int} = {} & \lambda_1 (H^\dagger H)(\Phi^\dagger \Phi) + \lambda_2 (\Phi^\dagger H)(H^\dagger \Phi) \\ & + \frac{1}{2}\lambda_3 [(\Phi^\dagger H)^2 + (H^\dagger \Phi)^2] + \frac{\lambda_{HT}}{2}(H^\dagger H)\mathrm{Tr}[\mathcal{T}^2] \\ & + \frac{\lambda_{\Phi\mathcal{T}}}{2}(\Phi^\dagger \Phi)\mathrm{Tr}[\mathcal{T}^2]. \end{aligned} \tag{3}$$

Following electroweak symmetry breaking (EWSB), the CP-even neutral component of H obtains VEV $v = 246$ GeV. On the other hand, the Z_2 and Z_2' ensures that the neutral components of Φ and $\mathcal{T}$ do not pick up VEVs, as stated before. The scalar fields can then be parametrized as

$$H = \begin{pmatrix} 0 \\ \frac{1}{\sqrt{2}}(v+h) \end{pmatrix}, \qquad \Phi = \begin{pmatrix} H^+ \\ \frac{1}{\sqrt{2}}(H_0 + iA_0) \end{pmatrix},$$
$$\mathcal{T} = \begin{pmatrix} \frac{1}{\sqrt{2}}T_0 - T^+ \\ -T^- - \frac{1}{\sqrt{2}}T_0 \end{pmatrix}, \tag{4}$$

and, after the EWSB, the masses of the physical scalars are given by

$$\begin{aligned} m_h^2 &= 2\lambda_H v^2, \\ m_{H^\pm}^2 &= \mu_\Phi^2 + \lambda_1 \frac{v^2}{2}, \\ m_{H_0}^2 &= \mu_\Phi^2 + (\lambda_1 + \lambda_2 + \lambda_3)\frac{v^2}{2}, \\ m_{A_0}^2 &= \mu_\Phi^2 + (\lambda_1 + \lambda_2 - \lambda_3)\frac{v^2}{2}, \\ m_{T_0,T^\pm}^2 &= M_T^2 + \frac{\lambda_{HT}}{2}v^2. \end{aligned} \tag{5}$$

In Eq. (5), $m_h = 125.09$ GeV [94] is the mass of SM Higgs. The fact that the scalars from the Φ multiplet have different masses at the tree level itself paves way for the possibility that H_0 is the lightest and is, therefore, a DM candidate. Unlike Φ, the charged and neutral members of $\mathcal{T}$ have degenerate masses at the tree level. However, thanks to radiative effects, this degeneracy is lifted at the one-loop level leading to the following mass splitting:

$$\Delta m = (m_{T^\pm} - m_{T_0})_{\text{1-loop}} = \frac{\alpha m_{T_0}}{4\pi}\left[f\left(\frac{M_W}{m_{T_0}}\right) - c_W^2 f\left(\frac{M_Z}{m_{T_0}}\right)\right], \tag{6}$$

where α is the fine structure constant, M_W and M_Z are the masses of the W and Z bosons, respectively, $c_W = \cos\theta_W = M_W/M_Z$, and $f(x) = -\frac{x}{4}[2x^3\ln(x) + (x^2-4)^{3/2}\ln(\frac{x^2-2-x\sqrt{x^2-4}}{2})]$, where $x = \frac{M_{W,Z}}{m_{T_0}}$. It turns out that in the limit $x \to 0$, i.e., $m_{T_0} \gg M_W$ or M_Z, $f(x) \to 2\pi x$ and Δm can be expressed as [95,96]

$$\Delta m = \frac{\alpha}{2} M_W \sin^2\frac{\theta_W}{2} = 166 \text{ MeV}. \tag{7}$$

One now gathers that T_0 is also stable and can be a DM candidate.

We now turn to identify the independent parameters in this scenario. A counting of parameters in the Lagrangian yields $\{\mu_H, \mu_\Phi, M_T, \lambda_H, \lambda_\Phi, \lambda_T, \lambda_1, \lambda_2, \lambda_3, \lambda_{HT}, \lambda_{\Phi T}\}$: 11 parameters. Now, μ_H is eliminated, demanding that the Higgs tadpole vanishes. At this level, we invoke $\lambda_L \equiv \frac{\lambda_1+\lambda_2+\lambda_3}{2}$ as an independent parameter that quantifies the $H_0 - H_0 - h$ portal interaction and, hence, is of profound importance in a Higgs portal DM scenario such as the IDM. Similarly, λ_{HT} parametrizes the strength of the $T_0 - T_0 - h$ portal coupling and is treated as an independent parameter henceforth. So is $\lambda_{\Phi T}$, since it parametrizes the $T_0 T_0 \to H_0 H_0$ conversion amplitude. Finally, μ_Φ, M_T, λ_1, λ_2, and λ_3 can be traded off with the inert masses and λ_L using

$$\mu_\Phi^2 = m_{H_0}^2 - \lambda_L v^2, \tag{8a}$$

$$M_T^2 = m_{T_0}^2 - \frac{\lambda_{HT}}{2}v^2, \tag{8b}$$

$$\lambda_1 = 2\lambda_L + \frac{2(m_{H^+}^2 - m_{H_0}^2)}{v^2}, \tag{8c}$$

$$\lambda_2 = \frac{m_{H_0}^2 + m_{A_0}^2 - 2m_{H^+}^2}{v^2}, \tag{8d}$$

$$\lambda_3 = \frac{m_{H_0}^2 - m_{A_0}^2}{v^2}. \tag{8e}$$

The independent parameters in the scalar sector are, therefore,

$$\{m_h, m_{H_0}, m_{A_0}, m_{H^\pm}, m_{T_0}, \lambda_L, \lambda_{HT}, \lambda_{\Phi T}, \lambda_H, \lambda_\phi, \lambda_T\}.$$

In passing, we add that λ_Φ and λ_T parametrize self-interaction within their respective inert sectors and, hence, are not phenomenologically that much relevant for the ensuing DM analysis. However, these couplings can indeed be constrained from the theoretical requirements of perturbativity, unitarity, and positivity of the scalar potential. A detailed discussion can be seen in Sec. III.

III. CONSTRAINTS

The present scenario is subject to the following theoretical and experimental constraints.

A. Theoretical constraints: Perturbativity, positivity of the scalar potential, and unitarity

The present model is deemed perturbative if the scalar quartic couplings obey $|\lambda_i| \leq 4\pi$. Furthermore, the gauge and Yukawa couplings must also satisfy $|g_i|, |y_i| \leq \sqrt{4\pi}$.

The introduction of additional scalars opens up additional directions in field space. The following conditions ensure that the potential remains bounded from below along each such direction:

$$\lambda_H, \quad \lambda_T, \quad \lambda_\Phi \geq 0, \tag{9a}$$

$$\lambda_{HT} + \sqrt{\frac{2}{3}\lambda_H \lambda_T} \geq 0, \tag{9b}$$

$$\lambda_1 + 2\sqrt{\lambda_H \lambda_\Phi} \geq 0, \tag{9c}$$

$$\lambda_1 + \lambda_2 - |\lambda_3| + 2\sqrt{\lambda_H \lambda_\Phi} \geq 0, \tag{9d}$$

$$\lambda_{\Phi T} + \sqrt{\frac{2}{3}\lambda_\Phi \lambda_T} \geq 0. \tag{9e}$$

Additional restrictions on the scalar potential come from unitarity. For this model, a couple of $2 \to 2$ scattering matrices can be constructed in the basis of neutral and singly charged two-particle states. Unitarity demands that the absolute value of each eigenvalue of these scattering matrices must be $\leq 8\pi$. An element of the scattering matrix is proportional to a quartic coupling in the high-energy limit. Following this prescription, one derives for this model

$$\begin{aligned}
&|\lambda_1 \pm \lambda_2| \leq 8\pi; \quad |\lambda_1 \pm \lambda_3| \leq 8\pi; \\
&\quad |\lambda_1 + 2\lambda_2 \pm \lambda_3| \leq 8\pi; \quad |\lambda_T| \leq 24\pi; \\
&|\lambda_{\Phi T}| \leq 8\pi; \quad |\lambda_{HT}| \leq 8\pi; \\
&\quad |\lambda_H + \lambda_\Phi \pm \sqrt{(\lambda_H - \lambda_\Phi)^2 + \lambda_2^2}| \leq 8\pi; \\
&|\lambda_H + \lambda_\Phi \pm \sqrt{(\lambda_H - \lambda_\Phi)^2 + \lambda_3^2}| \leq 8\pi.
\end{aligned} \tag{10}$$

Furthermore, since the present study discusses Higgs vacuum stability, the conditions of perturbativity, positivity of the scalar potential, and unitarity have to be met at each intermediate scale while evolving from the EW scale to a higher scale under the RG.

B. DM observables

For the present scenario to be a successful DM model, the thermal relic abundance it predicts must lie in the observed band. Adopting the latest result from the measurement of relic abundance by the Planck experiment, we demand from our model

$$0.119 \lesssim \Omega h^2 < 0.121. \tag{11}$$

Nonobservation of DM-nucleon scattering in the terrestrial experiments has put upper limits on the corresponding cross section as a function of the DM mass. We abide by in our study the bound on the spin-independent direct detection cross section from XENON-1T, the experiment predicting the most stringent bound.

C. LHC diphoton signal strength

The dominant amplitude for the $h \to \gamma\gamma$ in the SM reads

$$\mathcal{M}^{\rm SM}_{h\to\gamma\gamma} = \frac{4}{3} A_{1/2}\left(\frac{M_h^2}{4M_t^2}\right) + A_1\left(\frac{M_h^2}{4M_W^2}\right). \tag{12}$$

We have neglected the small effect of fermions other than the t quark in Eq. (12). The presence of additional charged scalars in the present framework implies modification to the $h \to \gamma\gamma$ amplitude with respect to the SM. This additional scalar contribution reads

$$M^S_{h\to\gamma\gamma} = \frac{\lambda_{hH^+H^-} v}{2m^2_{H^+}} A_0\left(\frac{m_h^2}{4m^2_{H^+}}\right) + \frac{\lambda_{hT^+T^-} v}{2m^2_{T^+}} A_0\left(\frac{m_h^2}{4m^2_{T^+}}\right), \tag{13}$$

where

$$\lambda_{hH^+H^-} = \lambda_1 v, \tag{14a}$$

$$\lambda_{hT^+T^-} = \lambda_{HT} v. \tag{14b}$$

The total amplitude and the decay width then become

$$\mathcal{M}_{h\to\gamma\gamma} = \mathcal{M}^{\rm SM}_{h\to\gamma\gamma} + \mathcal{M}^{\rm S}_{h\to\gamma\gamma}, \tag{15}$$

$$\Gamma_{h\to\gamma\gamma} = \frac{G_F \alpha^2 m_h^3}{128\sqrt{2}\pi^3} |\mathcal{M}_{h\to\gamma\gamma}|^2, \tag{16}$$

respectively, where G_F is the Fermi constant. The various loop functions are listed below [97]:

$$A_{1/2}(x) = \frac{2}{x^2}((x + (x-1)f(x)), \tag{17a}$$

$$A_1(x) = -\frac{1}{x^2}((2x^2 + 3x + 3(2x-1)f(x)), \tag{17b}$$

$$A_0(x) = -\frac{1}{x^2}(x - f(x)), \tag{17c}$$

with $f(x) = \arcsin^2(\sqrt{x}); \quad x \le 1$

$$= -\frac{1}{4}\left[\log\frac{1+\sqrt{1-x^{-1}}}{1-\sqrt{1-x^{-1}}} - i\pi\right]^2; \quad x > 1, \tag{17d}$$

where $A_{1/2}(x)$, $A_1(x)$, and $A_0(x)$ are loop functions corresponding to spin-$\frac{1}{2}$, spin-1, and spin-0 particles in the loop. The signal strength for the $\gamma\gamma$ channel is defined as

$$\mu_{\gamma\gamma} = \frac{\sigma(pp \to h)\mathrm{BR}(h \to \gamma\gamma)}{[\sigma(pp \to h)\mathrm{BR}(h \to \gamma\gamma)]_{\mathrm{SM}}}. \tag{18}$$

Given that inert multiplets do not modify the $pp \to h$ production,

$$\mu_{\gamma\gamma} = \frac{\mathrm{BR}(h \to \gamma\gamma)}{[\mathrm{BR}(h \to \gamma\gamma)]_{\mathrm{SM}}} \tag{19}$$

$$\simeq \frac{\Gamma^{\mathrm{SM}}_{h\to\gamma\gamma}}{\Gamma_{h\to\gamma\gamma}}. \tag{20}$$

In order to ensure that $\mu_{\gamma\gamma}$ lies within the experimental uncertainties, the analysis should respect the latest signal strength from ATLAS [98] and CMS [99]. The measured values of $\mu_{\gamma\gamma}$ are given by $\mu_{\gamma\gamma} = 0.99 \pm 0.14$ from ATLAS and $\mu_{\gamma\gamma} = 1.17 \pm 0.10$ from CMS. The constraints have been imposed at 2σ.

D. Disappearing charged track

The smallness of the mass splitting between T^+ and T_0 implies that the $T^+ \to T_0\pi^+$ decay width is tiny. The parent particle T^+ will, therefore, travel a macroscopic distance [$\mathcal{O}(1\ \mathrm{cm})$] before decaying, thereby leading to multiple hits in the LHC tracking devices. In addition, the π^+ would be too *soft* to be detected. As a result, a *disappearing charged track* (DCT) signal would be seen. The lighter T^+, the higher the $pp \to T^+T^-$ production cross section at the LHC and, hence, the higher the number of DCT events. It then follows that nonobservation of such events at the LHC would lead to lower bounds on the mass of T^+. It was shown recently [100] that nonobservation of DCT signals at the 13 TeV, integrated luminosity $(L) = 36\ \mathrm{fb}^{-1}$ excludes a real triplet scalar lighter than 275 GeV. The reach can extend to 590 and 745 GeV with $L = 300$ and $3000\ \mathrm{fb}^{-1}$, respectively. We have, therefore, maintained $m_{T^+} > 275$ GeV throughout the analysis in light of the current constraint.

E. Oblique parameters

The additional scalars present in this setup can induce potentially important contributions to the oblique (S, T, U) parameters. That is, for $X = S$, T, U, one can write

$$\Delta X = \Delta X_{\mathrm{ID}} + \Delta X_{\mathrm{IT}}, \tag{21}$$

where the subscript ID (IT) denotes the contribution from the inert doublet (triplet). We have for the inert doublet

$$\Delta S_{\mathrm{ID}} = \frac{1}{2\pi}\left[\frac{1}{6}\ln\left(\frac{m^2_{H_0}}{m^2_{H^\pm}}\right) - \frac{5}{36} + \frac{m^2_{H_0}m^2_{A_0}}{3(m^2_{A_0} - m^2_{H_0})^2} + \frac{m^4_{A_0}(m^2_{A_0} - 3m^2_{H_0})}{6(m^2_{A_0} - m^2_{H_0})^3}\ln\left(\frac{m^2_{A_0}}{m^2_{H_0}}\right)\right], \tag{22a}$$

$$\Delta T_{\mathrm{ID}} = \frac{1}{16\pi s^2_W M^2_W}[F(m^2_{H^+}, m^2_{H_0}) + F(m^2_{H^+}, m^2_{A_0}) - F(m^2_{H_0}, m^2_{A_0})], \tag{22b}$$

$$\Delta U_{\mathrm{ID}} = 0. \tag{22c}$$

In the above,

$$F(x,y) = \frac{x+y}{2} - \frac{xy}{x-y}\ln\left(\frac{x}{y}\right) \quad \text{for } x \neq y, \quad = 0 \quad \text{for } x = y. \tag{23}$$

For the inert triplet,

$$\Delta S_{\mathrm{IT}} = 0, \tag{24a}$$

$$\Delta T_{\mathrm{IT}} = \frac{1}{16\pi s^2_W M^2_W}F(m^2_{T^+}, m^2_{T_0}) \tag{24b}$$

$$\simeq \frac{(\Delta m)^2}{24\pi s^2_W M^2_W} \quad \text{since } \Delta m \ll m_{T_0}, \tag{24c}$$

$$\Delta U_{\mathrm{IT}} = -\frac{1}{3\pi}\left[m^4_{T_0}\ln\left(\frac{m^2_{T_0}}{m^2_{T^\pm}}\right)\frac{(3m^2_{T^\pm} - m^2_{T_0})}{(m^2_{T_0} - m^2_{T^\pm})^3} + \frac{5(m^4_{T_0} + m^4_{T^\pm}) - 22m^2_{T_0}m^2_{T^\pm}}{6(m^2_{T_0} - m^2_{T^\pm})^2}\right] \simeq \frac{\Delta m}{3\pi m_{T^\pm}}. \tag{24d}$$

The most updated bounds read [101]

$$\Delta S = 0.02 \pm 0.10, \quad \Delta T = 0.07 \pm 0.12, \quad \Delta U = 0.00 \pm 0.09. \tag{25}$$

The stated bounds have been imposed at 2σ in our analysis. A few comments are in order. First, the contribution of an inert real scalar triplet to the oblique parameters is found to be at most $\mathcal{O}\left(\frac{\Delta m}{m_{T_0}}\right)$ or further suppressed. The contributions are, therefore, negligible in comparison to the corresponding ones from the inert doublet. Second, a nonzero T parameter indicates that the ρ parameter deviates from unity at one loop (since the doublets and the VEV-less triplet present in this model predict $\rho = 1$ at tree level). However, ensuring that T stays within the stipulated bound is tantamount to obeying the ρ-parameter constraint.

IV. DARK MATTER PHENOMENOLOGY

The present setup, being a two-component DM scenario, has the discrete symmetry $Z_2 \times Z_2'$ that remains unbroken throughout and guarantees the stability of the DM candidates. To find the individual contributions to the relic density, one requires to evaluate the yields of both the DM species by solving coupled Boltzmann equations. In order to do so, first we identify all the relevant annihilation and coannihilation channels of both (we refer the reader to Refs. [52,63], where all such channels for IDM and ITM are listed, respectively). Apart from these, diagrams responsible for DM-DM conversion are shown in Fig. 1 assuming $m_{T_0} > m_{H_0}$. This interconversion of the two DM particles plays a significant role in our analysis and, in turn, makes the set of Boltzmann equations coupled. Next, to calculate the DM relic abundance, we implement the model file in LanHEP [102] and then pass the files generated in LanHEP to micrOMEGAS [103]. For inspecting the current scenario, we consider the all constraints discussed in Sec. III.

A. Relic density

In order to obtain the comoving number densities of both DM particles, one needs to solve a set of coupled Boltzmann equation in the present setup, as the conversion of one DM to another plays a nontrivial role. Because of the involvement of two DM particles, it is always better to redefine the usual x parameter from $\frac{m_{\rm DM}}{\tilde{T}}$ to $\frac{\mu_{\rm DM}}{\tilde{T}}$, where $\mu_{\rm DM}$ is nothing but the reduced mass expressed as $\mu_{\rm DM} = \frac{m_{H_0} m_{T_0}}{m_{H_0}+m_{T_0}}$, whereas $\tilde{T}$ represents the temperature of the Universe. Finally, we write the coupled Boltzmann equations in terms of parameter $x = \frac{\mu_{\rm DM}}{\tilde{T}}$ and the comoving number density $Y_{\rm DM} = n_{\rm DM}/s$ (s being the entropy density) redefined as y_i ($i = H_0, T_0$) via $y_i = 0.264 M_{\rm Pl}\sqrt{g_*}\mu Y_i$, as below[1]:

$$\frac{dy_{H_0}}{dx} = \frac{-1}{x^2}\Big[\langle\sigma v_{H_0H_0\to XX}\rangle(y_{H_0}^2 - (y_{H_0}^{EQ})^2) + \langle\sigma v_{H_0H_0\to T_0T_0}\rangle\left(y_{H_0}^2 - \frac{(y_{H_0}^{EQ})^2}{(y_{T_0}^{EQ})^2}y_{T_0}^2\right)\Theta(m_{H_0}-m_{T_0}) - \langle\sigma v_{T_0T_0\to H_0H_0}\rangle\left(y_{T_0}^2 - \frac{(y_{T_0}^{EQ})^2}{(y_{H_0}^{EQ})^2}y_{H_0}^2\right)\Theta(m_{T_0}-m_{H_0})\Big], \tag{26a}$$

$$\frac{dy_{T_0}}{dx} = \frac{-1}{x^2}\Big[\langle\sigma v_{T_0T_0\to XX}\rangle(y_{T_0}^2 - (y_{T_0}^{EQ})^2) + \langle\sigma v_{T_0T_0\to H_0H_0}\rangle\left(y_{T_0}^2 - \frac{(y_{T_0}^{EQ})^2}{(y_{H_0}^{EQ})^2}y_{H_0}^2\right)\Theta(m_{T_0}-m_{H_0}) - \langle\sigma v_{H_0H_0\to T_0T_0}\rangle\left(y_{H_0}^2 - \frac{(y_{H_0}^{EQ})^2}{(y_{T_0}^{EQ})^2}y_{T_0}^2\right)\Theta(m_{H_0}-m_{T_0})\Big]. \tag{26b}$$

One can relate y_i^{EQ} in the same way as y_i via $y_i^{EQ} = 0.264 M_{\rm Pl}\sqrt{g_*}\mu_{\rm DM}Y_i^{EQ}$, where Y_i^{EQ} is the equilibrium density Y_i^{EQ} defined in terms of $\mu_{\rm DM}$ as

$$Y_i^{EQ}(x) = 0.145\frac{g}{g_*}x^{3/2}\left(\frac{m_i}{\mu_{\rm DM}}\right)^{3/2}e^{-x(m_i/\mu_{\rm DM})}. \tag{27}$$

Here, $M_{\rm Pl} = 1.22 \times 10^{19}$ GeV, $g_* = 106.7$, $m_i = m_{H_0}, m_{T_0}$, X represents all the SM particles $H^\pm$, A_0, and $T^\pm$, and, finally, the thermally averaged effective annihilation cross section inclusive of both the annihilation and DM-DM conversion processes can be expressed as

$$\langle\sigma v\rangle = \frac{1}{8m_i^4\tilde{T}K_2^2(\frac{m_i}{\tilde{T}})}\int_{4m_i^2}^{\infty}\sigma(s-4m_i^2)\sqrt{s}K_1\left(\frac{\sqrt{s}}{\tilde{T}}\right)ds \tag{28}$$

and is evaluated at $\tilde{T}_f$. The freeze-out temperature $\tilde{T}_f$ can be derived by equating the DM interaction rate $\Gamma = n_{\rm DM}\langle\sigma v\rangle$ with the expansion rate of the Universe $H(\tilde{T}) \simeq \sqrt{\frac{\pi^2 g_*}{90}}\frac{T^2}{M_{\rm Pl}}$. In Eq. (28), $K_{1,2}(x)$ represents the modified Bessel functions. Finally, in Eq. (26), the Θ function is used in order to explain the conversion process (corresponding to Fig. 1) of one DM to another which strictly depends on the mass hierarchy of DM particles.

At this stage, it is perhaps pertinent to mention that $H^\pm$ (heavier than H_0) and $T^\pm$ (heavier than T_0) are expected to be in equilibrium with the thermal plasma by virtue of their electromagnetic interactions as well as their interactions with the Higgs. Apart from being in equilibrium, the H^+ can decay into $H_0 l^+\bar{\nu}$ and T^+ can decay to $T_0\pi^+$ via off-shell W bosons. Finally, A_0 being heavier than H_0 can always decay to H_0 and the SM fermions via an off-shell Z.

[1]We use the notation from a recent article on two-component DM [78].

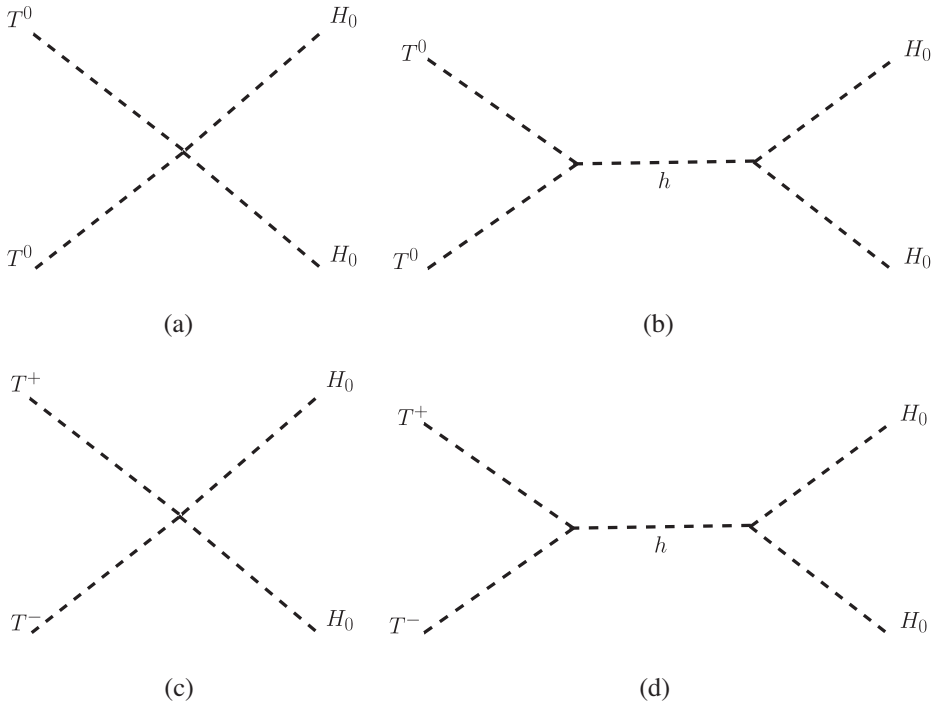

FIG. 1. DM-DM conversion channels, assuming $m_{T_0} > m_{H_0}$.

The heavier scalars within the dark multiplets are, thus, not cosmologically stable. These coupled equations now have to be solved numerically to find the asymptotic abundance of the DM particles, $y_i(\frac{\mu_{\rm DM}}{m_i}x_\infty)$, which can be further used to calculate the relic density:

$$\Omega_i h^2 = \frac{854.45\times 10^{-13}}{\sqrt{g_*}}\frac{m_i}{\mu_{\rm DM}}y_i\left(\frac{\mu_{\rm DM}}{m_i}x_\infty\right), \tag{29}$$

where x_∞ indicates a very large value of x after decoupling. The total DM relic abundance is then given as

$$\Omega_{\rm Total}h^2 = \Omega_{T_0}h^2 + \Omega_{H_0}h^2. \tag{30}$$

It is to be noted that the total relic abundance must satisfy the DM relic density obtained from Planck [28]:

$$\Omega_{\rm Total}h^2 = 0.1199 \pm 0.0027. \tag{31}$$

B. Direct and indirect detection

Experiments like LUX [90], PandaX-II [92,93], and Xenon-1T [91,104] look for signals of DM-nucleon scattering. And, nonobservation of the same have led to upper bounds on the DM-nucleon scattering cross section as a function of the DM mass. It must be added that, in principle, inelastic direct detection scatterings can also get triggered in case the mass gap between the DM and the next heavier particle within the multiplet is below ~150 keV [105]. Being a two-component DM scenario, in the present model both the DM particles would appear in direct search experiments. However, one should take into account the fact that direct detection cross sections of both are to be rescaled by the corresponding relic density fractions. Hence, the effective direct detection cross section of triplet scalar DM T_0 is given as [106]

$$\sigma_{T_0,\rm eff} = \frac{\Omega_{T_0}}{\Omega_{\rm Total}}\frac{\lambda_{HT}^2}{4\pi}\frac{1}{m_h^4}f^2\frac{m_N^4}{(m_{T_0}+m_N)^2}, \tag{32}$$

and similarly the effective direct detection cross section of H_0 is expressed as [44]

$$\sigma_{H_0,\rm eff} = \frac{\Omega_{H_0}}{\Omega_{\rm Total}}\frac{\lambda_L^2}{4\pi}\frac{1}{m_h^4}f^2\frac{m_N^4}{(m_{H_0}+m_N)^2}, \tag{33}$$

where m_N is the nucleon mass and λ_{HT} and λ_L are the quartic couplings involved in the DM-Higgs interaction. A recent estimate of the Higgs-nucleon coupling (f) gives $f = 0.32$ [107]. We provide the Feynman diagrams for the spin-independent elastic scattering of DM with a nucleon in Fig. 2.

On the other hand, indirect search experiments like Fermi-LAT [108] also offer promising prospects of detecting WIMP DM candidates. Annihilation of DM to SM particles, especially to photons and neutrinos, plays a crucial role here. Since photons and neutrinos are electrically neutral, they have a higher chance of reaching the detector without getting deflected. The effective indirect detection cross section $\sigma^{\rm ID}_{i,\rm eff}$ in a multicomponent DM setup relates to the computed cross section $\sigma^{\rm ID}_i$ as [43,109]

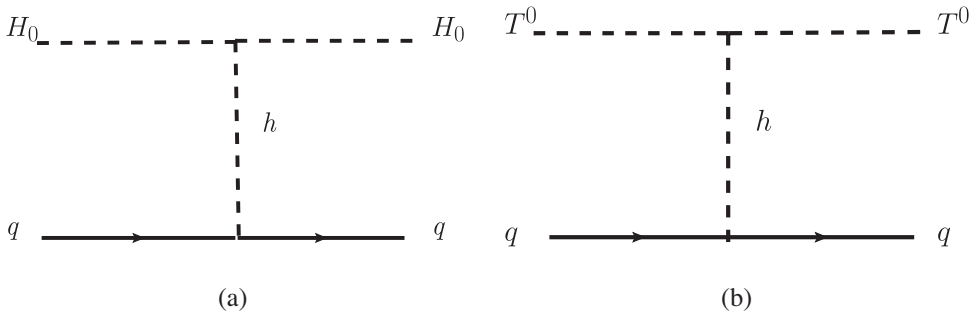

FIG. 2. Spin-independent elastic scattering of DM-nucleon.

$$\sigma^{\rm ID}_{i,\rm eff} = \left(\frac{\Omega_i}{\Omega_{\rm Total}}\right)^2 \sigma^{\rm ID}_i. \tag{34}$$

The exponent 2 in $(\frac{\Omega_i}{\Omega_{\rm Total}})^2$ in the case of indirect detection can be explained using the fact that there are two annihilating DM particles in the initial state as opposed to one in the case of direct detection. We demand that $\sigma^{\rm ID}_{i,\rm eff}$ obey the upper bound from Fermi-LAT for $i = H_0, T_0$.

C. Result

The phenomenologies of the single-component IDM [31–42] as well as ITM [53–59] are well known. Despite being allowed by the direct search experiments, both fail to predict the observed for a substantial range of the DM mass. While this underabundant region extends from M_W to 500 GeV for the IDM, the same is, in fact, larger for the ITM. In this case, the underabundant region extends till 1.8 TeV of the DM mass (irrespective of the choices of their Higgs portal couplings, as their impact on the relic density is subdominant) particularly because, apart from its usual annihilations to SM gauge bosons, it must coannihilate to the gauge bosons with the help of its charged partners $T^{\pm}$ (mass splitting is very small, i.e., $\Delta m = 166$ MeV). This, in turn, makes the effective annihilation cross section of the triplet DM quite large, hence leading to underabundance of the relic density for a wider range of the DM mass as compared to the IDM. We comment on the role of the portal coupling λ_{HT} here. The co(annihilations) are heavily gauge coupling driven, and the dependence on λ_{HT} is subleading. To show this, we plot the triplet relic density for $\lambda_{HT} = 0.1, 0.2, 1$ in the right panel in Fig. 3. It is seen that Ω_{T_0} for $\lambda_{HT} = 0.1, 0.2$ differ only slightly away from the h resonance (our region of interest in $m_{T_0} \gtrsim 750$ GeV). For $\lambda_{HT} = 1$, though there appears to be a sizable difference, we can still say that the role of the h-mediated annihilation is subleading compared to the gauge-driven annihilations. This can be understood from the following example. Increasing λ_{HT} from 0.2 to 1 increases the h-mediated annihilation cross section 25-fold. However, the relic density for $m_{T_0} = 1.8$ TeV drops only by a factor of $\sim$2. This shows that the contribution of the gauge-driven (co) annihilation is way higher. Despite this subleading impact of λ_{HT}, a large $\sim$1 value for the former can still deplete the relic density by $\simeq$50% (with respect to $\lambda_{HT} = 0.2$). This depletion is something we do not aim for and, therefore, restrict λ_{HT} in the [0.1, 0.2] interval henceforth. And, for such a choice, the $T_0T_0, T^+T^- \to H_0H_0$ conversion is dominated by the $T^+ - T^- - H_0 - H_0$ and $T_0 - T_0 - H_0 - H_0$ contact interactions and not by the s-channel h exchange.

In order to maximize the relic density from the inert doublet, we choose $m_{H^{\pm}} = m_{A_0}$. With $m_{H^{\pm}} \neq m_{A_0}$, this

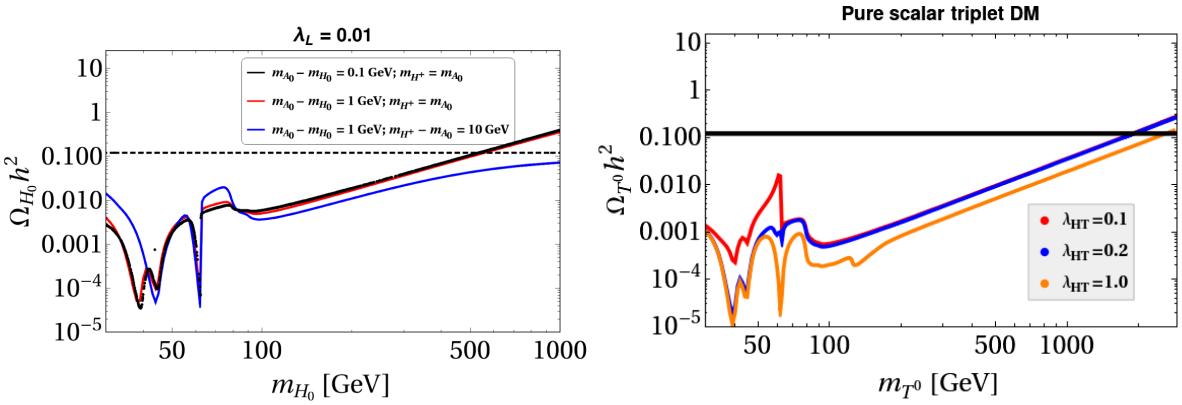

FIG. 3. Left panel: the relic density of the inert doublet for $m_{H^+} = m_{A_0}$ and $m_{H^+} = m_{A_0} + 10$ GeV. Right panel: variation of $\Omega_{T_0}h^2$ versus m_{T_0} for different values of λ_{HT}.

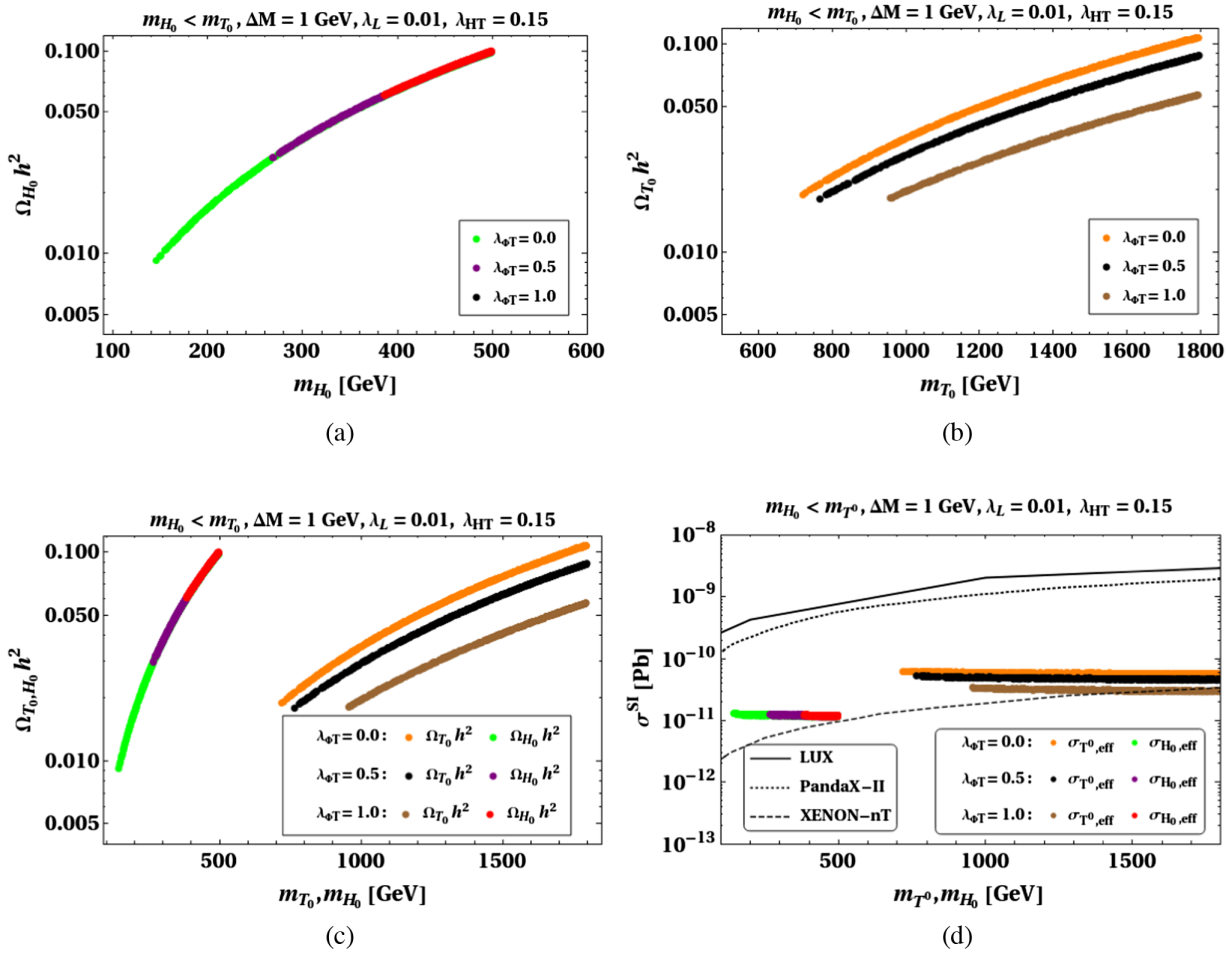

FIG. 4. Points that satisfy the correct total DM relic abundance for $\lambda_{HT} = 0.15$, $\lambda_L = 0.01$, $\Delta M = 1$ GeV, and different values of $\lambda_{\Phi T}$ while maintaining $m_{T_0} > m_{H_0}$ in the (a) $m_{H_0} - \Omega_{H_0} h^2$ plane and (b) $m_{T_0} - \Omega_{T_0} h^2$ plane. (c) combines the plots in (a) and (b). (d) shows the corresponding spin-independent DM-nucleon scattering cross sections corresponding to the points in (c). Limits from direct detection experiments are shown in black solid (LUX), dotted (PandaX-II), and dashed lines (XENONnT).

contribution will be accordingly less. We have demonstrated this in the left panel in Fig. 3 by comparing the relic densities corresponding to $m_{H^+} = m_{A_0}$ and $m_{H^+} = m_{A_0} + 10$ GeV. The gap thereby made in the total relic density will then have to be compensated by the scalar triplet. Given a heavier T_0 tends to predict a higher Ω_{T_0}, the parameter region for $\lambda_2 \neq \lambda_3$ would prefer an accordingly heavier T_0. This is contrary to our objective of accomplishing a *lighter* T_0 (by "lighter," we imply lighter than what is seen in the single-component triplet dark matter scenario).

In the present study, we aim to find out if interconversion (which depends on their mass hierarchy, though) of one DM species to another can possibly revive such mass regions of IDM and ITM that are known to yield underabundant thermal relic abundance. As stated before, the relevant parameters that would control the study are m_{H_0}, m_{A_0}, $m_{H^\pm}$, λ_L, λ_{HT}, and $\lambda_{\Phi T}$. For the analysis purpose, we stick only to mass regime 100 GeV $\leq m_{H_0} \leq$ 500 GeV and 100 GeV $\leq m_{T_0} \leq$ 2000 GeV for the doublet and the triplet, respectively. As the Higgs portal couplings of both DMs do not play a very significant role in obtaining the correct total relic density for the given choice of the parameter space, we fixed the portal couplings $\lambda_L = 0.01$ and $\lambda_{HT} = 0.15$. Even though the role of the portal couplings is subleading in the DM phenomenology, they play a nontrivial role in stabilizing the electroweak vacuum which will be discussed in detail in Sec. V.

In Figs. 4(a) and 4(b), we show the variation of the individual relic density contributions, $\Omega_{H_0} h^2$ and $\Omega_{T_0} h^2$, against their respective masses, m_{H_0} and m_{T_0}, such that the total relic density ($\Omega_{\text{Total}} h^2$) defined in Eq. (30) satisfies the Planck limit [28]. A combined plot is Fig. 4(c). In the same plot, we also show the effect of different choices of the coupling $\lambda_{\Phi T}$ (involved in DM-DM conversion as shown in Fig. 1) on the parameter space. Here, we choose three different values of $\lambda_{\Phi T}$ for illustration, i.e., $\lambda_{\Phi T} = 0$, 0.5, and 1.0.

The respective variations of the relic densities versus the DM masses with different $\lambda_{\Phi T}$ are indicated by (i) orange (for T_0) and green (for H_0) patches for $\lambda_{\Phi T} = 0$, (ii) black

(for T_0) and purple (for H_0) patches for $\lambda_{\Phi T} = 0.5$, and (iii) brown (for T_0) and red (for H_0) patches for $\lambda_{\Phi T} = 1.0$. Here, for our analysis purpose, we also define mass splitting among the inert doublet components as $\Delta M = m_{H^\pm} - m_{H_0} = m_{A_0} - m_{H_0}$ and fix its value at 1 GeV. Such a choice of the ΔM is motivated from the fact that the maximum contribution from the single-component IDM to relic density can be obtained for such small mass splittings only [31–42]. It is to be noted that the inelastic direct detection processes are ruled out in the IDM for such a mass splitting. In the case of the inert triplet also, the mass gap $m_{T^+} - m_{T_0} = 166$ MeV is too large to trigger the W-mediated inelastic scattering $T_0 T^+ \to \bar{q} q'$.

We would like to elucidate on Fig. 4 a bit. One must note that $\Omega_{H_0} h^2$ and $\Omega_{T_0} h^2$ in the figure obey $\Omega_{H_0} h^2 + \Omega_{T_0} h^2 =$ observed relic $\simeq 0.12$ (the variation within the *PLANCK* band ignored here for the sake of understanding). For instance, for $\lambda_{\Phi T} = 0.5$, $\Omega_{H_0} h^2$ for a particular m_{H_0} can be read from the violet curve. The corresponding $\Omega_{T_0} h^2$ is then approximately equal to 0.12 $\Omega_{H_0} h^2$, and one can then read the corresponding m_{T_0} value on the X axis. This implies that the relic densities of the rightmost point on the violet curve and the leftmost point on the black curve add up to $\simeq 0.12$. This is how Fig. 4 should be read.[2]

To understand the nontriviality of the conversion coupling in the present setup, we begin with the case where $\lambda_{\Phi T} = 0$. Note that with $\lambda_{\Phi T} = 0$, although conversion via the process shown in Fig. 1(a) does not contribute, the processes $T^+ T^-$, $T_0 T_0 \to H_0 H_0$ can still take place due to the nonzero values of λ_L and λ_{HT} via the one in Fig. 1(b). Here, we observe that when $\Omega_{T_0} h^2$ is small (corresponding to the lowest point of the orange patch), the dominant contribution toward the total relic density comes from $\Omega_{H_0} h^2$ (topmost point of the green patch which lies below the red patch) so as to satisfy the total relic density with the Planck limit. Similarly, the farthest point on the orange patch corresponds to the lowest point of the green one. As an example, for $m_{T_0} = 785$ GeV we get $\Omega_{T_0} h^2 = 0.019$ (almost 15% of the total relic density); the rest of the 85% of the total relic density comes from $\Omega_{H_0} h^2$, which corresponds to a single point on the green patch with $m_{H_0} = 498$ GeV and $\Omega_{H_0} h^2 = 0.098$.

Upon turning on the conversion coupling (say, $\lambda_{\Phi T} = 0.5$), a shift in the relic densities of both the DM candidates is observed (see the black and the purple patches in Fig. 4). The reason behind this is easy to understand. When the conversion coupling is switched on, the T_0 starts converting to H_0 and, hence, the relic density of the T_0 decreases, whereas we observe an upward shift for the relic density Ω_{H_0} (the purple patch). A similar behavior is observed for $\lambda_{\Phi T} = 1.0$, where the relic density of T_0 is further decreased and the relic density of H_0 is increased; we notice that the red patch has now become much smaller. This is because the maximum contribution toward the total relic density from T_0 can at most be 53% (with $m_{T_0} = 1790$ GeV, $\Omega_{T_0} h^2 = 0.060$) which, in turn, requires $\Omega_{H_0} h^2 = 0.056$ (the rest of the 47% contribution toward the total relic density) for $m_{H_0} = 387$ GeV, leading to a shrinking in the red patch. In Fig. 4(d), we plot the effective direct detection cross section of both DMs with respect to their respective masses and compare it with the experimental results obtained from LUX [90], PandaX-II [92,93], and XENONnT [110] for different values of $\lambda_{\Phi T}$ [similar to Fig. 4(a)]. Here, it is interesting to point out that, although the current setup is allowed from the constraints coming from present direct search experiments like LUX [90] and PandaX-II [92,93], the parameter space of the setup can come in tension with the XENONnT projections. However, this is actually a positive finding, since this renders the model testable and, hence, falsifiable in a future experiment. Considering Fig. 4(a) and the bounds from the present direct search results from Fig. 4(d) together, we can conclude that the parameter space under consideration is allowed from both the relic density as well as the direct detection constraints. For better understanding, we also tabulate the result discussed above in Table II for three different choices of the conversion couplings $\lambda_{\Phi T} = 0.0$, 0.5, and 1.0.

TABLE II. Table showing the relic densities for certain sample mass values for different $\lambda_{\Phi T}$. We have taken $\lambda_L = 0.01$ and $\lambda_{HT} = 0.15$.

$\lambda_{\Phi T}$	m_{H_0} [GeV]	m_{T_0} [GeV]	$\Omega_{H_0} h^2$	$\Omega_{T_0} h^2$
0.0	500	730	0.0981	0.0192
	147	1799	0.0092	0.1070
0.5	500	770	0.0988	0.0180
	280	1799	0.0320	0.0875
1.0	500	1000	0.0993	0.0194
	388	1799	0.0606	0.0568

Finally, in Fig. 5, we incorporate parameter region plots in the $m_{H_0} - m_{T_0}$ plane for $\Delta M = 1$ (left panel) and 5 GeV (right panel). All the points in this case are allowed by the relic density and direct detection constraints. The effect of the conversion coupling discussed in Fig. 4(a) becomes prominent in Fig. 5. Looking at the left panel in Fig. 5, one may notice that almost the entire desert mass regime of the single-component IDM and m_{T_0} in the range 700 GeV $\leq m_{T_0} \leq 2$ TeV (the relic density of a $Y = 0$ triplet being underabundant for $m_{T_0} < 1.8$ TeV) now becomes allowed in the two-component setup, thanks to DM-DM conversion. However, for the higher value $\Delta M = 5$ GeV, we observe in the right panel that m_{T_0} shifts toward the heavier side. This happens because, with the increase in the mass

[2]This approach is based on Ref. [44].

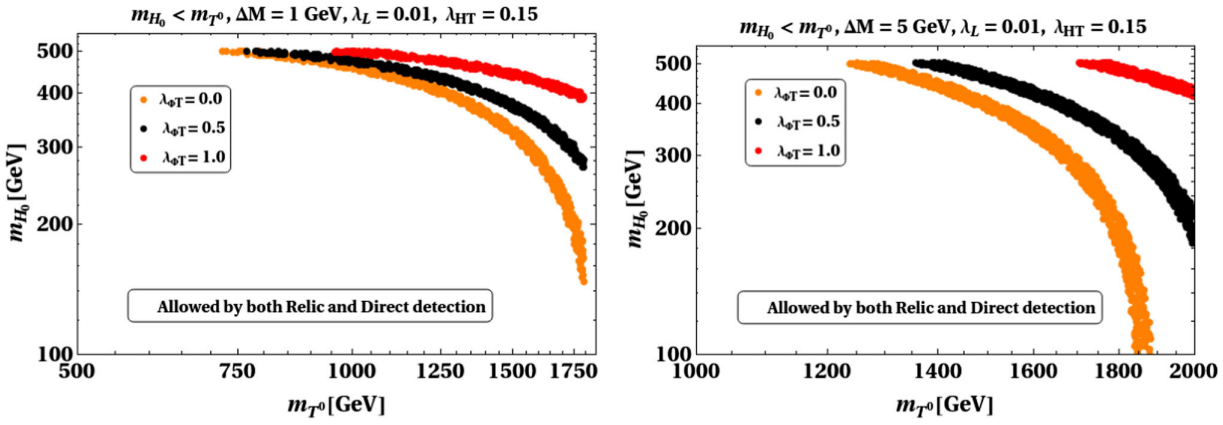

FIG. 5. All the points which satisfy the correct total DM relic abundance and are also allowed by direct detection for different values of $\lambda_{\Phi T}$ while maintaining $m_{T_0} > m_{H_0}$ for $\lambda_{HT} = 0.15$ and (a) $\Delta M = 1$ GeV and (b) $\Delta M = 5$ GeV in the $m_{H_0} - m_{T_0}$ plane.

splitting among the inert doublet components, the contribution of Φ to the total relic density decreases, and, hence, in order for total relic density to satisfy the Planck limit, the triplet contribution has to increase, which can result only from an accordingly larger mass of the triplet DM.

Although the effect of the Higgs portal coupling λ_{HT} is subleading in the present scenario, a small effect of its variation can be observed in the parameter space when we vary the mass splitting among the inert doublet components. We try to demonstrate this subleading behavior via a heat plot in Fig. 6. For a fixed m_{T_0}, the annihilation rate of the scalar triplet increases upon increasing λ_{HT}, thereby causing $\Omega_{T_0}h^2$ to drop, albeit mildly. Since the total relic density is demanded to lie in the Planck band, $\Omega_{H_0}h^2$ must accordingly increase to fill the gap. And that is possible

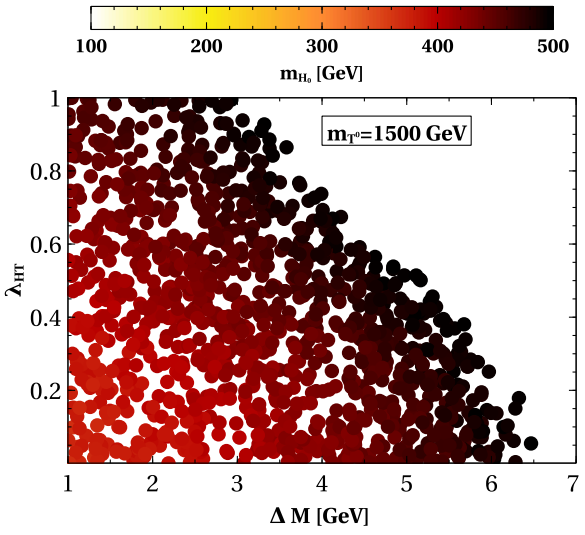

FIG. 6. Variation of triplet-Higgs portal coupling (λ_{HT}) with inert doublet mass splitting (ΔM) for a fixed value of $m_{T_0} = 1500$ GeV. The color bar shows the variation with m_{H_0}.

only for a higher inert doublet DM mass. And since the larger the m_{H_0}, the darker the shade, one expects a darkening of the points as one moves up the λ_{HT} axis. This is exactly what is observed in Fig. 6, where a gradual darkening is seen as one moves up from the bottom left to the top left corner. On the other hand, as ΔM increases, $\Omega_{H_0}h^2$ tends to decrease for a given m_{H_0}. If λ_{HT} is held fixed, one then has to increase m_{H_0} to maintain the original $\Omega_{H_0}h^2$. A darkening of the points is then expected as one moves toward the right of the ΔM axis. An inspection of the figure corroborates this when such a darkening is immediately seen.

Prior to ending this section, we comment on the consequences of an $m_{H_0} > m_{T_0}$ hierarchy. Here, the processes responsible for DM conversion will now be reversed, and the inert doublet is expected to be responsible for the production of the second dark matter T_0, i.e., $H_0H_0 \to T_0T_0$. As mentioned before, a sub-TeV scalar triplet always leads to an underabundant relic due to high co(annihilation) rates to gauge boson final states. Given that we restrict $m_{H_0} < 500$ GeV in this study, demanding $m_{H_0} > m_{T_0}$ at the same time implies that even the $H_0H_0 \to T_0T_0$ conversion does not suffice to generate the observed relic. Therefore, the $m_{H_0} > m_{T_0}$ hierarchy is not appealing from the two-component DM perspective, and we shall not consider it any further.

V. EW VACUUM STABILITY AND COMBINED ANALYSIS

This section discusses the role of the additional scalar multiplets in (meta)stabilizing the EW vacuum. For high field values, i.e., $h \gg v$, the RG improved effective potential for this scenario can be expressed as [4]

$$V_H^{\text{eff}} \simeq \frac{\lambda_H^{\text{eff}}(h)}{4} h^4, \tag{35}$$

TABLE III. Sample points predicting a total relic density within the Planck band that are also allowed by the theoretical, direct detection, indirect detection, and diphoton signal strength constraints. All masses and mass splittings are in GeV.

SP	m_{H_0}	m_{T_0}	λ_{HT}	ΔM	$\mu_{\gamma\gamma}$	$\Omega_{T_0}h^2$	$\Omega_{H_0}h^2$	$\sigma_{T_0,\text{eff}}$ (pb)	$\sigma_{H_0,\text{eff}}$ (pb)	$\sigma^{\text{ID}}_{T_0,\text{eff}}$ (cm^3/s)	$\sigma^{\text{ID}}_{H_0,\text{eff}}$ (cm^3/s)
SP1	400	1426	0.1	1	0.999	0.056	0.064	2.01×10^{-11}	1.2×10^{-11}	7.1×10^{-28}	1.2×10^{-26}
SP2	400	1426	0.15	1	0.999	0.056	0.064	4.5×10^{-11}	1.2×10^{-11}	7.1×10^{-28}	1.2×10^{-26}
SP3	400	1426	0.2	1	0.999	0.056	0.064	8.1×10^{-11}	1.2×10^{-11}	7.0×10^{-28}	1.2×10^{-26}
SP4	400	1670	0.15	5	0.997	0.076	0.044	4.5×10^{-11}	8.0×10^{-12}	2.1×10^{-27}	5.3×10^{-27}
SP5	400	1856	0.15	10	0.994	0.093	0.025	4.5×10^{-11}	4.6×10^{-12}	5.9×10^{-27}	1.7×10^{-27}

where $\lambda_H^{\text{eff}}(\mu)=\lambda_H(\mu)+\lambda_H^{\text{SM,eff}}(\mu)+\lambda_H^{\Phi,\text{eff}}(\mu)+\lambda_H^{T,\text{eff}}(\mu)$. Here, $\lambda_H^{\text{SM,eff}}(\mu)$ is the contribution coming from the SM fields to λ_H, whereas $\lambda_H^{\Phi,\text{eff}}(\mu)$ and $\lambda_H^{T,\text{eff}}(\mu)$ are the contributions from Φ and T, respectively. The EW boundary scale from which the couplings start evolving is chosen to be the t-quark pole mass $M_t=173.34$ GeV. All the running couplings are to be evaluated at a scale $\mu=h$ in Eq. (35). One derives the following:

$$\lambda_H^{\Phi,\text{eff}}(\mu)=e^{4\Gamma(\mu)}\frac{1}{16\pi^2}\left[2\frac{\lambda_1^2}{4}\left(\ln\frac{\lambda_1}{2}-\frac{3}{2}\right)+\frac{(\lambda_1+\lambda_2+\lambda_3)^2}{4}\left(\ln\frac{\lambda_1+\lambda_2+\lambda_3}{2}-\frac{3}{2}\right)+\frac{(\lambda_1+\lambda_2-\lambda_3)^2}{4}\left(\ln\frac{\lambda_1+\lambda_2-\lambda_3}{2}-\frac{3}{2}\right)\right], \tag{36}$$

$$\lambda_H^{T,\text{eff}}(\mu)=e^{4\Gamma(\mu)}\frac{1}{16\pi^2}\left[\frac{3\lambda_{HT}^2}{4}\left(\ln\frac{\lambda_{HT}}{2}-\frac{3}{2}\right)\right]. \tag{37}$$

Here, $\Gamma(\mu)=\int_{M_t}^{\mu}\gamma(\mu')\text{d}\ln(\mu')$ and $\gamma(\mu)$ denotes the anomalous dimension of the Higgs field [3]. By virtue of such quantum effects, a second minima can show up at high energy scales. The condition $\lambda_H^{\text{eff}}(\mu)>0$ ensures that the EW minimum is deeper than the second minimum, that is, a *stable* EW vacuum. On the other hand, $\lambda_H^{\text{eff}}(\mu)<0$ implies that the second minimum is deeper. The fate of the EW vacuum in this case is decided by computing the probability of tunneling to the second vacuum. The expression for the tunneling probability is given by

$$\mathcal{P}_T=(\mu_B T_U)^4 e^{-8\pi^2/3\lambda_H(\mu_B)}. \tag{38}$$

In Eq. (38), T_U is the age of the Universe, and μ_B denotes the scale at which the tunneling probability is maximized, determined from $\beta_{\lambda_H}(\mu_B)=0$. The EW vacuum is *metastable* if the tunneling lifetime is greater than the Universe's age. With this, one obtains the following criterion on $\lambda_H^{\text{eff}}(\mu)$:

$$\lambda_H^{\text{eff}}(\mu)>\frac{-0.065}{1-\ln(v/\mu_B)}. \tag{39}$$

The following boundary values are then taken for the SM Yukawa and gauge couplings [3][3]:

$$y_t(M_t)=0.93690+0.00556\times(M_t-173.34)-0.00042\times(\alpha_s(M_Z)-0.1184)/0.0007, \tag{40a}$$

$$g_1(M_t)=0.35830+0.00011\times(M_t-173.34)-0.00020\times(M_W-80.384)/0.014, \tag{40b}$$

$$g_2(M_t)=0.64779+0.00004\times(M_t-173.34)+0.00011\times(M_W-80.384)/0.014, \tag{40c}$$

$$g_3(M_t)=1.1666-0.00046\times(M_t-173.34)+0.00314\times(\alpha_s(M_Z)-0.1184)/0.0004. \tag{40d}$$

We take $M_W=80.384$ GeV and $\alpha_s(M_Z)=0.1184$. The input values of λ_1, λ_2, and λ_3 are determined using Eqs. (8c)–(8e).

[3]Heaviness of the IDM and ITM masses implies that their possible threshold contributions to the gauge and Yukawa couplings are negligible.

The expression for β_{λ_H} in Eq. (A1a) tells us that the quartic couplings the vacuum instability (or metastability) scale is sensitive to are λ_{1-3} and λ_{HT}. The sample points (SPs) listed in Table III demonstrate this sensitivity. We choose $\lambda_L=0.01$, $\lambda_{\Phi T}=0.5$, $\lambda_\phi=0.001$, and $\lambda_T=0.001$ throughout the analysis using the RG. It is noted that the SP1–3 differ only in their values of λ_{HT}. Since (co)annihilation in the triplet sector is heavily driven by

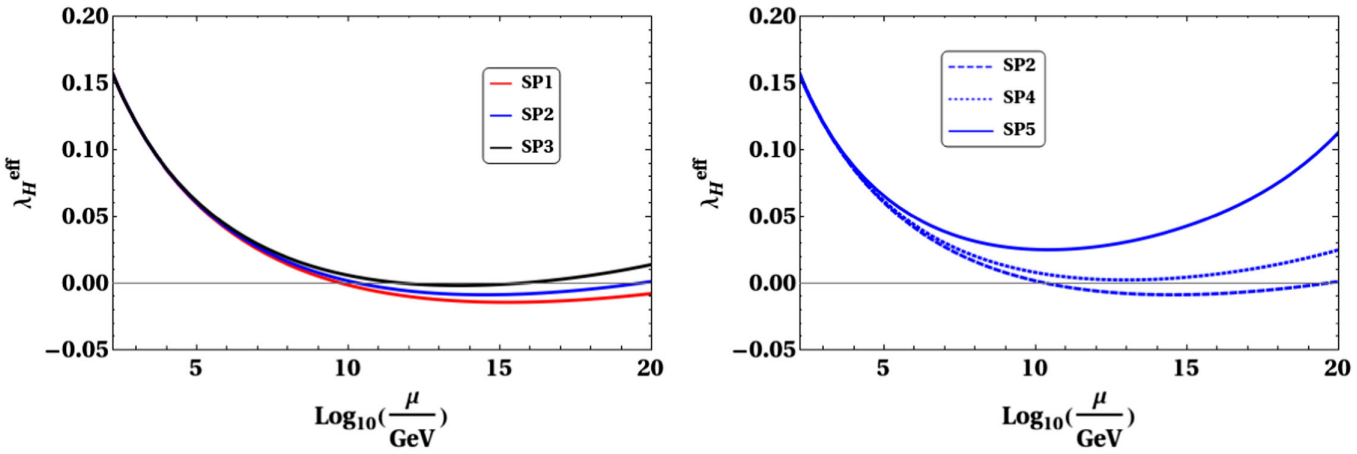

FIG. 7. RG evolution of $\lambda_H^{\rm eff}$ for the SPs. In the left panel for SP1, SP2, and SP3 the values are for $\{\lambda_1, \lambda_2, \lambda_3\} = \{0.046, -0.013 - 0.013\}$, while in the right panel for SP4 $\{\lambda_1, \lambda_2, \lambda_3\} = \{0.153, -0.066, -0.066\}$ and for SP5 $\{\lambda_1, \lambda_2, \lambda_3\} = \{0.287, -0.134, -0.134\}$.

gauge interactions, tuning λ_{HT} in the interval [0.1, 0.2] changes Ω_{T_0} only slightly. The corresponding RG trajectories of $\lambda_H^{\rm eff}$ are shown in the left panel in Fig. 7. It is seen that, though $\lambda_H^{\rm eff}$ turns negative in each case, it remains within the metastable band. In addition, the larger the input value of λ_{HT}, the higher the scale at which $\lambda_H^{\rm eff}$ turns negative. As mentioned before, this is solely due to the presence of the $\mathcal{O}(\lambda_{HT}^2)$ term in β_{λ_H}. While SP4 and SP5 are primarily characterized by their values of ΔM, the m_{T_0} values are also different for each. This is because a decrease in Ω_{H_0} that inevitably occurs with an increasing ΔM in these sample points is counterbalanced by an increased contribution from the triplet, something, in turn, achieved by appropriately raising m_{T_0}. Now, with λ_L fixed, increasing ΔM accordingly increases the magnitudes of λ_{1-3} at the EW scale. This, in turn, generates an upward push to the RG trajectory of $\lambda_H^{\rm eff}$ via the λ_{1-3}-dependent terms in β_{λ_H}. Since SP2, SP4, and SP5 feature different ΔM values for the same λ_{HT}, we show the corresponding RG evolution curves in the right panel in Fig. 7 in order to confirm the impact of changing ΔM. A metastable EW vacuum is identified for $\Delta M = 1$ GeV. Increasing the same to $\Delta M = 5$ and 10 GeV stabilizes the same up to the Planck scale.

The bands corresponding to metastable and stable EW vacuum sketched in the $m_{T_0} - m_{H_0}$ plane are shown in Fig. 8. Also, the parameter region predicting the requisite relic density and compatible with the direct detection constraints is overlaid on the same. Upon inspection, it is seen that the parameter plane mostly favors metastability over stability for $\lambda_{HT} = 0.1$ and $\Delta M = 5$ GeV. And this is attributed to the EW scale values of λ_1, λ_2, λ_3, and λ_{HT} that are not sizable enough to stabilize the vacuum till $M_{\rm Pl}$ for most of the $m_{T_0} - m_{H_0}$ plane. In fact, a stable vacuum is ruled out for $m_{H_0} \lesssim 480$ GeV. With increasing λ_{HT} to 0.15, the band corresponding to stability expands to include $m_{H_0} \gtrsim 360$ GeV. This is expected for the following reason. For a higher λ_{HT}, accordingly smaller $|\lambda_1|$, $|\lambda_2|$, and $|\lambda_3|$ suffice to ensure a stable vacuum up to $M_{\rm Pl}$. And with λ_L and ΔM fixed, smaller $|\lambda_1|$, $|\lambda_2|$, and $|\lambda_3|$ imply a smaller m_{H_0}. We also remark that the parameter region compatible with the DM constraints changes only slightly with this change in λ_{HT}, since the (co)annihilations of the triplet scalars are mostly driven by the gauge interactions. Demanding the requisite relic abundance rules out $m_{T_0} \lesssim 1.35$ TeV for $\Delta M = 5$ GeV.

As illustrated before in Fig. 7, increasing ΔM while keeping λ_L unchanged aids vacuum stability by increasing the magnitudes of λ_1, λ_2, and λ_3. In other words, with a higher ΔM, the requisite magnitudes of these quartic couplings at the input scale required to stabilize the EW vacuum up to the Planck scale can be achieved for an accordingly lower m_{H_0}. This is concurred by the plot with $\lambda_{HT} = 0.1$ and $\Delta M = 10$ GeV, in which case the stability band includes $m_{H_0} \gtrsim 240$ GeV. In addition, the DM-compatible region also changes appreciably with respect to $\Delta M = 5$ GeV. With now a higher mass splitting in the inert doublet sector, Ω_{H_0} diminishes. Heavier triplet scalars are needed to fill up the deficit in relic density compared to what occurs for $\Delta M = 5$ GeV. This is the reason why the DM-compatible region shifts toward the right in the $m_{T_0} - m_{H_0}$ plane when switching from $\Delta M = 5$ to 10 GeV. The observed relic abundance, in fact, obviates $m_{T_0} \lesssim 1.7$ TeV for $\Delta M = 10$ GeV. Once again, we would like to contrast this finding with the stand-alone IDM. In the present IDM + ITM setup, a smaller ΔM is required to stabilize the vacuum till the Planck scale compared to what would be required in the case of the stand-alone IDM. This is expected on the grounds of an additional bosonic contribution coming from the triplet in the case of the IDM + ITM. To cite an example parameter point, for $M_H = 250$ GeV, $\lambda_L = 0.01$, a stable EW vacuum within

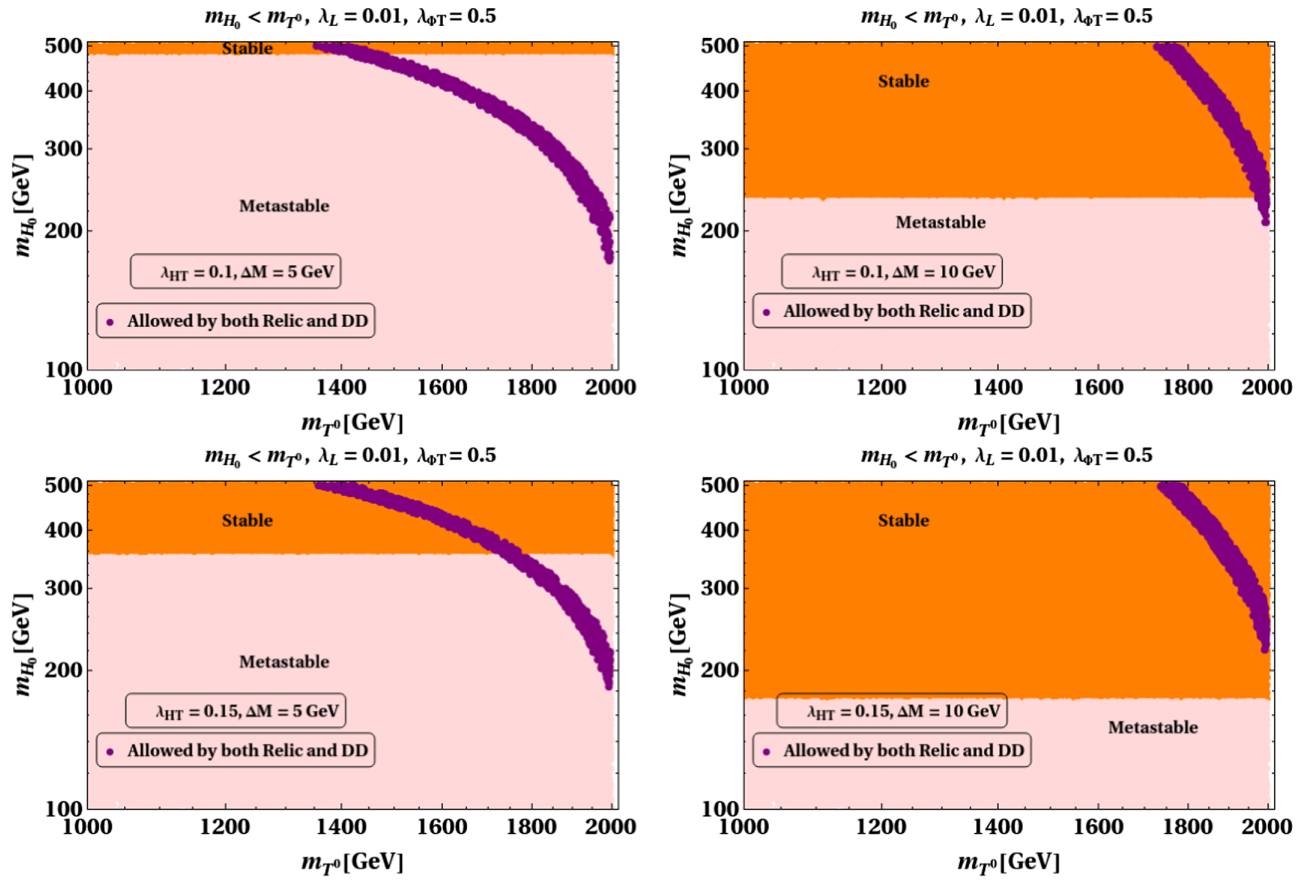

FIG. 8. Parameter region compatible with (meta)stable vacuum and the DM observables in the $m_{T_0} - m_{H_0}$ plane. The orange (pink) bands correspond to stability (metastability). The blue region is allowed by the DM constraints.

the stand-alone IDM mandates the higher mass gap $\Delta M \gtrsim 14$ GeV. And we reiterate that the relic density also remains underabundant for the same. Therefore, the introduction of an additional inert triplet significantly modifies the analyses of both DM phenomenology and EW vacuum stability. While the IDM desert region now becomes compatible with the observed relic density, it also predicts a stable EW vacuum all the way up to the Planck scale for a lower ΔM.

VI. CONCLUSIONS

Despite its popularity, the stand-alone inert scalar doublet fails to account for the observed thermal relic abundance in the desert region, i.e., 100 GeV $< M_{\rm DM} <$ 500 GeV. Similarly, a $Y = 0$ inert triplet is seen to yield only underabundant relic density for $M_{\rm DM} < 1.8$ TeV. In this work, we extend the scalar sector of the SM by both the aforementioned multiplets and impose a $Z_2 \times Z_2'$ symmetry so that the scalar doublet and triplet constitute two different dark sectors. A two-component DM scenario is consequently realized with the neutral CP-even scalar from each multiplet as a DM candidate. The quartic coupling $\lambda_{\Phi T}$, that controls the rate of DM-DM conversion, emerges as a crucial parameter. Also important in the context of DM phenomenology is the mass splitting between the inert scalars on which the corresponding relic density is sensitive to. For an appropriate choice of the relevant model parameters, we demonstrate how DM-DM conversion is instrumental in generating the observed relic densities for the doublet scalar mass in the desert region and a sub-TeV triplet scalar. Moreover, this observation is found to be consistent with the latest DD bound.

We also compute the one-loop RG equations for the present framework and subsequently discuss (meta)stability of the EW vacuum. Demanding a stable vacuum up to the Planck scale in addition to the requisite relic density further restricts the mass regions of interest. For instance, a stable vacuum till the Planck scale disfavors sub-TeV triplet DM for the mass splitting among the doublet scalars not exceeding 10 GeV. In all, we show that DM-DM conversion in the present multicomponent DM model can lead to an explanation of the observed relic density in specific mass regions that are otherwise known to yield underabundance in the corresponding single-component cases. That the aforementioned observation is compatible with a stable vacuum up to the Planck scale is a major upshot of this analysis. Lastly, we add that the present scenario also bears an interesting discovery potential at LHC. It is, in

fact, more prospective to probe a *lighter* charged triplet scalar via the disappearing charge track at the detector. This direction warrants a separate investigation in the near future.

ACKNOWLEDGMENTS

N. C. is financially supported by IISc (Indian Institute of Science, Bangalore, India) through the C. V. Raman post-doctoral fellowship. N. C. also acknowledges support from DST, India, under Grant No. IFA19-PH237 (INSPIRE Faculty Award).

APPENDIX: BETA FUNCTIONS

The one-loop beta functions for the quartic couplings can be split as $\beta_{\lambda_i} = \beta^S_{\lambda_i} + \beta^F_{\lambda_i} + \beta^G_{\lambda_i}$. Then

$$16\pi^2\beta^S_{\lambda_H} = 24\lambda_H^2 + 2\lambda_1^2 + 2\lambda_1\lambda_2 + \lambda_2^2 + \lambda_3^2 + \frac{3}{2}\lambda_{HT}^2, \quad \text{(A1a)}$$

$$16\pi^2\beta^S_{\lambda_\phi} = 24\lambda_\phi^2 + 2\lambda_1^2 + 2\lambda_1\lambda_2 + \lambda_2^2 + \lambda_3^2 + \frac{3}{2}\lambda_{\Phi T}^2, \quad \text{(A1b)}$$

$$16\pi^2\beta^S_{\lambda_T} = \frac{11}{3}\lambda_T^2 + 12\lambda_{HT}^2 + 12\lambda_{\Phi T}^2, \quad \text{(A1c)}$$

$$16\pi^2\beta^S_{\lambda_1} = 4\lambda_1^2 + 2\lambda_2^2 + 2\lambda_3^2 + 12\lambda_1\lambda_H + 4\lambda_2\lambda_H + 12\lambda_1\lambda_\phi + 4\lambda_2\lambda_\phi + 3\lambda_{HT}\lambda_{\Phi T}, \quad \text{(A1d)}$$

$$16\pi^2\beta^S_{\lambda_2} = 4\lambda_2^2 + 8\lambda_3^2 + 8\lambda_1\lambda_2 + 4\lambda_2\lambda_H + 4\lambda_2\lambda_\phi, \quad \text{(A1e)}$$

$$16\pi^2\beta^S_{\lambda_3} = 8\lambda_1\lambda_3 + 12\lambda_2\lambda_3 + 4\lambda_3\lambda_H + 4\lambda_3\lambda_\phi, \quad \text{(A1f)}$$

$$16\pi^2\beta^S_{\lambda_{HT}} = 4\lambda_{HT}^2 + 12\lambda_H\lambda_{HT} + 4\lambda_1\lambda_{\Phi T} + 2\lambda_2\lambda_{\Phi T} + \frac{5}{3}\lambda_{HT}\lambda_T, \quad \text{(A1g)}$$

$$16\pi^2\beta^S_{\lambda_{\Phi T}} = 4\lambda_{\Phi T}^2 + 12\lambda_\phi\lambda_{\Phi T} + 4\lambda_1\lambda_{HT} + 2\lambda_2\lambda_{HT} + \frac{5}{3}\lambda_{\Phi T}\lambda_T. \quad \text{(A1h)}$$

$$16\pi^2\beta^F_{\lambda_H} = 12\lambda_H y_t^2 - 6y_t^4, \quad \text{(A2a)}$$

$$16\pi^2\beta^F_{\lambda_\phi} = 0, \quad \text{(A2b)}$$

$$16\pi^2\beta^F_{\lambda_T} = 0, \quad \text{(A2c)}$$

$$16\pi^2\beta^F_{\lambda_1} = 6\lambda_1 y_t^2, \quad \text{(A2d)}$$

$$16\pi^2\beta^F_{\lambda_2} = 6\lambda_2 y_t^2, \quad \text{(A2e)}$$

$$16\pi^2\beta^F_{\lambda_3} = 6\lambda_3 y_t^2, \quad \text{(A2f)}$$

$$16\pi^2\beta^F_{\lambda_{HT}} = 6\lambda_{HT} y_t^2, \quad \text{(A2g)}$$

$$16\pi^2\beta^F_{\lambda_{\Phi T}} = 0. \quad \text{(A2h)}$$

$$16\pi^2\beta^G_{\lambda_H} = -3\lambda_H(g_1^2 + 3g_2^2) + \frac{3}{8}(g_1^4 + 3g_2^4 + 2g_1^2g_2^2), \quad \text{(A3a)}$$

$$16\pi^2\beta^G_{\lambda_\phi} = -3\lambda_\phi(g_1^2 + 3g_2^2) + \frac{3}{8}(g_1^4 + 3g_2^4 + 2g_1^2g_2^2), \quad \text{(A3b)}$$

$$16\pi^2\beta^G_{\lambda_T} = -24\lambda_T g_2^2 + 72g_2^4, \quad \text{(A3c)}$$

$$16\pi^2\beta^G_{\lambda_1} = -3\lambda_1(g_1^2 + 3g_2^2) + \frac{3}{4}(g_1^4 + 3g_2^4 - 2g_1^2g_2^2), \quad \text{(A3d)}$$

$$16\pi^2\beta^G_{\lambda_2} = -3\lambda_2(g_1^2 + 3g_2^2) + 3g_1^2g_2^2, \quad \text{(A3e)}$$

$$16\pi^2\beta^G_{\lambda_3} = -3\lambda_3(g_1^2 + 3g_2^2), \quad \text{(A3f)}$$

$$16\pi^2\beta^G_{\lambda_{HT}} = -\lambda_{HT}\left(\frac{3}{2}g_1^2 + \frac{33}{2}g_2^2\right) + 6g_2^4, \quad \text{(A3g)}$$

$$16\pi^2\beta^G_{\lambda_{\Phi T}} = -\lambda_{\Phi T}\left(\frac{3}{2}g_1^2 + \frac{33}{2}g_2^2\right) + 6g_2^4. \quad \text{(A3h)}$$

The t-Yukawa evolves according to

$$16\pi^2\beta_{y_t} = \frac{9}{2}y_t^3 - y_t\left(\frac{17}{12}g_1^2 + \frac{9}{4}g_2^2 + 8g_3^2\right). \quad \text{(A4)}$$

Finally, the gauge couplings have the following beta functions:

$$16\pi^2\beta_{g_1} = 7g_1^3, \quad \text{(A5a)}$$

$$16\pi^2\beta_{g_2} = -\frac{8}{3}g_2^3, \quad \text{(A5b)}$$

$$16\pi^2\beta_{g_3} = 16\pi^2\beta^{\rm SM}_{g_3} = -7g_3^3. \quad \text{(A5c)}$$

[1] S. Chatrchyan *et al.* (CMS Collaboration), Observation of a new boson at a mass of 125 GeV with the CMS experiment at the LHC, Phys. Lett. B **716**, 30 (2012).

[2] G. Aad *et al.* (ATLAS Collaboration), Observation of a new particle in the search for the Standard Model Higgs boson with the ATLAS detector at the LHC, Phys. Lett. B **716**, 1 (2012).

[3] D. Buttazzo, G. Degrassi, P. P. Giardino, G. F. Giudice, F. Sala, A. Salvio, and A. Strumia, Investigating the near-criticality of the Higgs boson, J. High Energy Phys. 12 (2013) 089.

[4] G. Degrassi, S. Di Vita, J. Elias-Miro, J. R. Espinosa, G. F. Giudice, G. Isidori, and A. Strumia, Higgs mass and vacuum stability in the Standard Model at NNLO, J. High Energy Phys. 08 (2012) 098.

[5] Y. Tang, Vacuum stability in the standard model, Mod. Phys. Lett. A **28**, 1330002 (2013).

[6] J. Ellis, J. R. Espinosa, G. F. Giudice, A. Hoecker, and A. Riotto, The probable fate of the standard model, Phys. Lett. B **679**, 369 (2009).

[7] J. Elias-Miro, J. R. Espinosa, G. F. Giudice, G. Isidori, A. Riotto, and A. Strumia, Higgs mass implications on the stability of the electroweak vacuum, Phys. Lett. B **709**, 222 (2012).

[8] J. Elias-Miro, J. R. Espinosa, G. F. Giudice, H. M. Lee, and A. Strumia, Stabilization of the electroweak vacuum by a scalar threshold effect, J. High Energy Phys. 06 (2012) 031.

[9] N. Haba, K. Kaneta, and R. Takahashi, Planck scale boundary conditions in the standard model with singlet scalar dark matter, J. High Energy Phys. 04 (2014) 029.

[10] N. Khan and S. Rakshit, Study of electroweak vacuum metastability with a singlet scalar dark matter, Phys. Rev. D **90**, 113008 (2014).

[11] V. V. Khoze, C. McCabe, and G. Ro, Higgs vacuum stability from the dark matter portal, J. High Energy Phys. 08 (2014) 026.

[12] N. Khan and S. Rakshit, Constraints on inert dark matter from the metastability of the electroweak vacuum, Phys. Rev. D **92**, 055006 (2015).

[13] M. Gonderinger, Y. Li, H. Patel, and M. J. Ramsey-Musolf, Vacuum stability, perturbativity, and scalar singlet dark matter, J. High Energy Phys. 01 (2010) 053.

[14] M. Gonderinger, H. Lim, and M. J. Ramsey-Musolf, Complex scalar singlet dark matter: Vacuum stability and phenomenology, Phys. Rev. D **86**, 043511 (2012).

[15] W. Chao, M. Gonderinger, and M. J. Ramsey-Musolf, Higgs vacuum stability, neutrino mass, and dark matter, Phys. Rev. D **86**, 113017 (2012).

[16] E. Gabrielli, M. Heikinheimo, K. Kannike, A. Racioppi, M. Raidal, and C. Spethmann, Towards completing the standard model: Vacuum stability, EWSB and dark matter, Phys. Rev. D **89**, 015017 (2014).

[17] N. Chakrabarty, U. K. Dey, and B. Mukhopadhyaya, High-scale validity of a two-Higgs doublet scenario: A study including LHC data, J. High Energy Phys. 12 (2014) 166.

[18] I. Chakraborty and A. Kundu, Two-Higgs doublet models confront the naturalness problem, Phys. Rev. D **90**, 115017 (2014).

[19] N. Chakrabarty, D. K. Ghosh, B. Mukhopadhyaya, and I. Saha, Dark matter, neutrino masses and high scale validity of an inert Higgs doublet model, Phys. Rev. D **92**, 015002 (2015).

[20] P. Ghosh, A. K. Saha, and A. Sil, Study of electroweak vacuum stability from extended Higgs portal of dark matter and neutrinos, Phys. Rev. D **97**, 075034 (2018).

[21] S. Bhattacharya, P. Ghosh, T. N. Maity, and T. S. Ray, Mitigating direct detection bounds in non-minimal Higgs portal scalar dark matter models, J. High Energy Phys. 10 (2017) 088.

[22] I. Garg, S. Goswami, K. Vishnudath, and N. Khan, Electroweak vacuum stability in presence of singlet scalar dark matter in TeV scale seesaw models, Phys. Rev. D **96**, 055020 (2017).

[23] A. Dutta Banik, A. K. Saha, and A. Sil, Scalar assisted singlet doublet fermion dark matter model and electroweak vacuum stability, Phys. Rev. D **98**, 075013 (2018).

[24] D. Borah, R. Roshan, and A. Sil, Sub-TeV singlet scalar dark matter and electroweak vacuum stability with vector like fermions, Phys. Rev. D **102**, 075034 (2020).

[25] V. C. Rubin and W. K. Ford, Jr., Rotation of the Andromeda Nebula from a spectroscopic survey of emission regions, Astrophys. J. **159**, 379 (1970).

[26] D. Clowe, M. Bradac, A. H. Gonzalez, M. Markevitch, S. W. Randall, C. Jones, and D. Zaritsky, A direct empirical proof of the existence of dark matter, Astrophys. J. Lett. **648**, L109 (2006).

[27] C. L. Bennett *et al.* (WMAP Collaboration), Nine-year Wilkinson Microwave Anisotropy Probe (WMAP) observations: Final maps and results, Astrophys. J. Suppl. Ser. **208**, 20 (2013).

[28] N. Aghanim *et al.* (Planck Collaboration), Planck 2018 results. VI. Cosmological parameters, Astron. Astrophys. **641**, A6 (2020).

[29] P. Athron *et al.* (GAMBIT Collaboration), Status of the scalar singlet dark matter model, Eur. Phys. J. C **77**, 568 (2017).

[30] N. G. Deshpande and E. Ma, Pattern of symmetry breaking with two Higgs doublets, Phys. Rev. D **18**, 2574 (1978).

[31] L. Lopez Honorez, E. Nezri, J. F. Oliver, and M. H. G. Tytgat, The inert doublet model: An archetype for dark matter, J. Cosmol. Astropart. Phys. 02 (2007) 028.

[32] L. Lopez Honorez and C. E. Yaguna, The inert doublet model of dark matter revisited, J. High Energy Phys. 09 (2010) 046.

[33] A. Belyaev, G. Cacciapaglia, I. P. Ivanov, F. Rojas-Abatte, and M. Thomas, Anatomy of the inert two Higgs doublet model in the light of the LHC and non-LHC dark matter searches, Phys. Rev. D **97**, 035011 (2018).

[34] S. Choubey and A. Kumar, Inflation and dark matter in the inert doublet model, J. High Energy Phys. 11 (2017) 080.

[35] L. Lopez Honorez and C. E. Yaguna, A new viable region of the inert doublet model, J. Cosmol. Astropart. Phys. 01 (2011) 002.

[36] A. Ilnicka, M. Krawczyk, and T. Robens, Inert doublet model in light of LHC run I and astrophysical data, Phys. Rev. D **93**, 055026 (2016).

[37] A. Arhrib, Y.-L. S. Tsai, Q. Yuan, and T.-C. Yuan, An updated analysis of inert Higgs doublet model in light of

the recent results from LUX, PLANCK, AMS-02 and LHC, J. Cosmol. Astropart. Phys. 06 (2014) 030.
[38] Q.-H. Cao, E. Ma, and G. Rajasekaran, Observing the dark scalar doublet and its impact on the Standard-Model Higgs boson at colliders, Phys. Rev. D **76**, 095011 (2007).
[39] E. Lundstrom, M. Gustafsson, and J. Edsjo, The inert doublet model and LEP II limits, Phys. Rev. D **79**, 035013 (2009).
[40] M. Gustafsson, S. Rydbeck, L. Lopez-Honorez, and E. Lundstrom, Status of the inert doublet model and the role of multileptons at the LHC, Phys. Rev. D **86**, 075019 (2012).
[41] J. Kalinowski, W. Kotlarski, T. Robens, D. Sokolowska, and A. F. Zarnecki, Benchmarking the inert doublet model for e^+e^- colliders, J. High Energy Phys. 12 (2018) 081.
[42] A. Bhardwaj, P. Konar, T. Mandal, and S. Sadhukhan, Probing inert doublet model using jet substructure with multivariate analysis, Phys. Rev. D **100**, 055040 (2019).
[43] S. Bhattacharya, P. Ghosh, A. K. Saha, and A. Sil, Two component dark matter with inert Higgs doublet: Neutrino mass, high scale validity and collider searches, J. High Energy Phys. 03 (2020) 090.
[44] D. Borah, R. Roshan, and A. Sil, Minimal two-component scalar doublet dark matter with radiative neutrino mass, Phys. Rev. D **100**, 055027 (2019).
[45] V. Keus, S. F. King, S. Moretti, and D. Sokolowska, Dark matter with two inert doublets plus one Higgs doublet, J. High Energy Phys. 11 (2014) 016.
[46] V. Keus, S. F. King, S. Moretti, and D. Sokolowska, Observable heavy Higgs dark matter, J. High Energy Phys. 11 (2015) 003.
[47] A. Cordero-Cid, J. Hernandez-Sanchez, V. Keus, S. F. King, S. Moretti, D. Rojas, and D. Sokolowska, *CP* violating scalar dark matter, J. High Energy Phys. 12 (2016) 014.
[48] N. Chakrabarty, High-scale validity of a model with three-Higgs-doublets, Phys. Rev. D **93**, 075025 (2016).
[49] A. Aranda, D. Hernández-Otero, J. Hernández-Sanchez, V. Keus, S. Moretti, D. Rojas-Ciofalo, and T. Shindou, Z_3 symmetric inert $(2+1)$-Higgs-doublet model, Phys. Rev. D **103**, 015023 (2021).
[50] V. Keus, Dark *CP*-violation through the *Z*-portal, Phys. Rev. D **101**, 073007 (2020).
[51] D. Borah and A. Gupta, New viable region of an inert Higgs doublet dark matter model with scotogenic extension, Phys. Rev. D **96**, 115012 (2017).
[52] S. Bhattacharya, N. Chakrabarty, R. Roshan, and A. Sil, Multicomponent dark matter in extended $U(1)_{B-L}$: Neutrino mass and high scale validity, J. Cosmol. Astropart. Phys. 04 (2020) 013.
[53] T. Araki, C. Q. Geng, and K. I. Nagao, Dark matter in inert triplet models, Phys. Rev. D **83**, 075014 (2011).
[54] O. Fischer and J. J. van der Bij, Multi-singlet and singlet-triplet scalar dark matter, Mod. Phys. Lett. A **26**, 2039 (2011).
[55] O. Fischer and J. J. van der Bij, The scalar singlet-triplet dark matter model, J. Cosmol. Astropart. Phys. 01 (2014) 032.
[56] N. Khan, Exploring the hyperchargeless Higgs triplet model up to the Planck scale, Eur. Phys. J. C **78**, 341 (2018).
[57] S. Jangid and P. Bandyopadhyay, Distinguishing inert Higgs doublet and inert triplet scenarios, Eur. Phys. J. C **80**, 715 (2020).
[58] B. Barman, P. Ghosh, F. S. Queiroz, and A. K. Saha, Scalar multiplet dark matter in a fast expanding universe: Resurrection of the desert region, Phys. Rev. D **104**, 015040 (2021).
[59] N. F. Bell, M. J. Dolan, L. S. Friedrich, M. J. Ramsey-Musolf, and R. R. Volkas, A real triplet-singlet extended Standard Model: Dark matter and collider phenomenology, J. High Energy Phys. 04 (2021) 098.
[60] P. Bandyopadhyay and A. Costantini, Obscure Higgs boson at colliders, Phys. Rev. D **103**, 015025 (2021).
[61] B. Ait-Ouazghour and M. Chabab, The Higgs potential in 2HDM extended with a real triplet scalar: A roadmap, Int. J. Mod. Phys. A **36**, 2150131 (2021).
[62] A. Goudelis, B. Herrmann, and O. Stl, Dark matter in the inert doublet model after the discovery of a Higgs-like boson at the LHC, J. High Energy Phys. 09 (2013) 106.
[63] A. Dutta Banik, R. Roshan, and A. Sil, Two component singlet-triplet scalar dark matter and electroweak vacuum stability, Phys. Rev. D **103**, 075001 (2021).
[64] Q.-H. Cao, E. Ma, J. Wudka, and C. P. Yuan, Multipartite dark matter, arXiv:0711.3881.
[65] A. Biswas, D. Majumdar, A. Sil, and P. Bhattacharjee, Two component dark matter: A possible explanation of 130 GeV γ-ray line from the galactic centre, J. Cosmol. Astropart. Phys. 12 (2013) 049.
[66] S. Bhattacharya, A. Drozd, B. Grzadkowski, and J. Wudka, Two-component dark matter, J. High Energy Phys. 10 (2013) 158.
[67] L. Bian, R. Ding, and B. Zhu, Two component Higgs-Portal dark matter, Phys. Lett. B **728**, 105 (2014).
[68] S. Esch, M. Klasen, and C. E. Yaguna, A minimal model for two-component dark matter, J. High Energy Phys. 09 (2014) 108.
[69] A. Karam and K. Tamvakis, Dark matter and neutrino masses from a scale-invariant multi-Higgs portal, Phys. Rev. D **92**, 075010 (2015).
[70] A. Karam and K. Tamvakis, Dark matter from a classically scale-invariant $SU(3)_X$, Phys. Rev. D **94**, 055004 (2016).
[71] S. Bhattacharya, P. Poulose, and P. Ghosh, Multipartite interacting scalar dark matter in the light of updated LUX data, J. Cosmol. Astropart. Phys. 04 (2017) 043.
[72] A. Dutta Banik, M. Pandey, D. Majumdar, and A. Biswas, Two component WIMP–FImP dark matter model with singlet fermion, scalar and pseudo scalar, Eur. Phys. J. C **77**, 657 (2017).
[73] A. Ahmed, M. Duch, B. Grzadkowski, and M. Iglicki, Multi-component dark matter: The vector and fermion case, Eur. Phys. J. C **78**, 905 (2018).
[74] J. Herrero-Garcia, A. Scaffidi, M. White, and A. G. Williams, On the direct detection of multi-component dark matter: Sensitivity studies and parameter estimation, J. Cosmol. Astropart. Phys. 11 (2017) 021.
[75] J. Herrero-Garcia, A. Scaffidi, M. White, and A. G. Williams, On the direct detection of multi-component dark matter: Implications of the relic abundance, J. Cosmol. Astropart. Phys. 01 (2019) 008.

[76] A. Poulin and S. Godfrey, Multicomponent dark matter from a hidden gauged SU(3), Phys. Rev. D **99**, 076008 (2019).
[77] M. Aoki and T. Toma, Boosted self-interacting dark matter in a multi-component dark matter model, J. Cosmol. Astropart. Phys. 10 (2018) 020.
[78] S. Bhattacharya, P. Ghosh, and N. Sahu, Multipartite dark matter with scalars, Fermions and signatures at LHC, J. High Energy Phys. 02 (2019) 059.
[79] M. Aoki, D. Kaneko, and J. Kubo, Multicomponent dark matter in radiative seesaw models, Front. Phys. **5**, 53 (2017).
[80] B. Barman, S. Bhattacharya, and M. Zakeri, Multipartite dark matter in $SU(2)_N$ extension of Standard Model and signatures at the LHC, J. Cosmol. Astropart. Phys. 09 (2018) 023.
[81] S. Chakraborti, A. Dutta Banik, and R. Islam, Probing multicomponent extension of inert doublet model with a vector dark matter, Eur. Phys. J. C **79**, 662 (2019).
[82] F. Elahi and S. Khatibi, Multi-component dark matter in a non-Abelian dark sector, Phys. Rev. D **100**, 015019 (2019).
[83] A. Biswas, D. Borah, and D. Nanda, Type III seesaw for neutrino masses in $U(1)_{B-L}$ model with multi-component dark matter, J. High Energy Phys. 12 (2019) 109.
[84] D. Nanda and D. Borah, Connecting light Dirac neutrinos to a multi-component dark matter scenario in gauged $B-L$ model, Eur. Phys. J. C **80**, 557 (2020).
[85] T. N. Maity and T. S. Ray, Exchange driven freeze out of dark matter, Phys. Rev. D **101**, 103013 (2020).
[86] S. Khalil, S. Moretti, D. Rojas-Ciofalo, and H. Waltari, Multi-component dark matter in a simplified E_6SSM model, Phys. Rev. D **102**, 075039 (2020).
[87] G. Blanger, A. Pukhov, C. E. Yaguna, and A. Zapata, The Z_5 model of two-component dark matter, J. High Energy Phys. 09 (2020) 030.
[88] C. H. Nam, D. Van Loi, L. X. Thuy, and P. Van Dong, Multicomponent dark matter in noncommutative $B-L$ gauge theory, J. High Energy Phys. 12 (2020) 029.
[89] A. Dutta Banik, R. Roshan, and A. Sil, Neutrino mass and asymmetric dark matter: Study with inert Higgs doublet and high scale validity, J. Cosmol. Astropart. Phys. 03 (2021) 037.
[90] D. S. Akerib *et al.* (LUX Collaboration), Results from a Search for Dark Matter in the Complete LUX Exposure, Phys. Rev. Lett. **118**, 021303 (2017).
[91] E. Aprile *et al.* (XENON Collaboration), Dark Matter Search Results from a One Ton-Year Exposure of XENON1T, Phys. Rev. Lett. **121**, 111302 (2018).
[92] A. Tan *et al.* (PandaX-II Collaboration), Dark Matter Results from First 98.7 Days of Data from the PandaX-II Experiment, Phys. Rev. Lett. **117**, 121303 (2016).
[93] X. Cui *et al.* (PandaX-II Collaboration), Dark Matter Results From 54-Ton-Day Exposure of PandaX-II Experiment, Phys. Rev. Lett. **119**, 181302 (2017).
[94] D. de Florian *et al.* (LHC Higgs Cross Section Working Group), *Handbook of LHC Higgs Cross Sections: 4. Deciphering the Nature of the Higgs Sector*, edited by D. de Florian, C. Grojean, F. Maltoni, C. Mariotti, A. Nikitenko, M. Pieri, P. Savard, M. Schumacher, and R. Tanaka, Vol. 2.
[95] M. Sher, Charged leptons with nanosecond lifetimes, Phys. Rev. D **52**, 3136 (1995).
[96] M. Cirelli, N. Fornengo, and A. Strumia, Minimal dark matter, Nucl. Phys. **B753**, 178 (2006).
[97] A. Djouadi, The anatomy of electro-weak symmetry breaking. II. The Higgs bosons in the minimal supersymmetric model, Phys. Rep. **459**, 1 (2008).
[98] M. Aaboud *et al.* (ATLAS Collaboration), Measurements of Higgs boson properties in the diphoton decay channel with 36 fb^{-1} of pp collision data at $\sqrt{s} = 13$ TeV with the ATLAS detector, Phys. Rev. D **98**, 052005 (2018).
[99] A. M. Sirunyan *et al.* (CMS Collaboration), Combined measurements of Higgs boson couplings in proton–proton collisions at $\sqrt{s} = 13$ TeV, Eur. Phys. J. C **79**, 421 (2019).
[100] C.-W. Chiang, G. Cottin, Y. Du, K. Fuyuto, and M. J. Ramsey-Musolf, Collider probes of real triplet scalar dark matter, J. High Energy Phys. 01 (2021) 198.
[101] P. Zyla *et al.* (Particle Data Group), Review of particle physics, Prog. Theor. Exp. Phys. **2020**, 083C01 (2020).
[102] A. Semenov, LanHEP: A package for automatic generation of Feynman rules from the Lagrangian. Version 3.2, Comput. Phys. Commun. **201**, 167 (2016).
[103] G. Bélanger, F. Boudjema, A. Pukhov, and A. Semenov, micrOMEGAs4.1: Two dark matter candidates, Comput. Phys. Commun. **192**, 322 (2015).
[104] E. Aprile *et al.* (XENON Collaboration), First Dark Matter Search Results from the XENON1T Experiment, Phys. Rev. Lett. **119**, 181301 (2017).
[105] C. Arina, F.-S. Ling, and M. H. G. Tytgat, IDM and iDM or the inert doublet model and inelastic dark matter, J. Cosmol. Astropart. Phys. 10 (2009) 018.
[106] S. Yaser Ayazi and S. M. Firouzabadi, Footprint of triplet scalar dark matter in direct, indirect search and invisible Higgs decay, Cogent Phys. **2**, 1047559 (2015).
[107] J. Giedt, A. W. Thomas, and R. D. Young, Dark Matter, the CMSSM and Lattice QCD, Phys. Rev. Lett. **103**, 201802 (2009).
[108] M. L. Ahnen *et al.* (MAGIC and Fermi-LAT Collaborations), Limits to dark matter annihilation cross-section from a combined analysis of MAGIC and Fermi-LAT observations of dwarf satellite galaxies, J. Cosmol. Astropart. Phys. 02 (2016) 039.
[109] A. Betancur, G. Palacio, and A. Rivera, Inert doublet as multicomponent dark matter, Nucl. Phys. **B962**, 115276 (2020).
[110] E. Aprile *et al.* (XENON Collaboration), Projected WIMP sensitivity of the XENONnT dark matter experiment, J. Cosmol. Astropart. Phys. 11 (2020) 031.